The Local Group

Fiducial Radius of the LG is about 1.0 Mpc: zero-velocity or radius of turn-around.

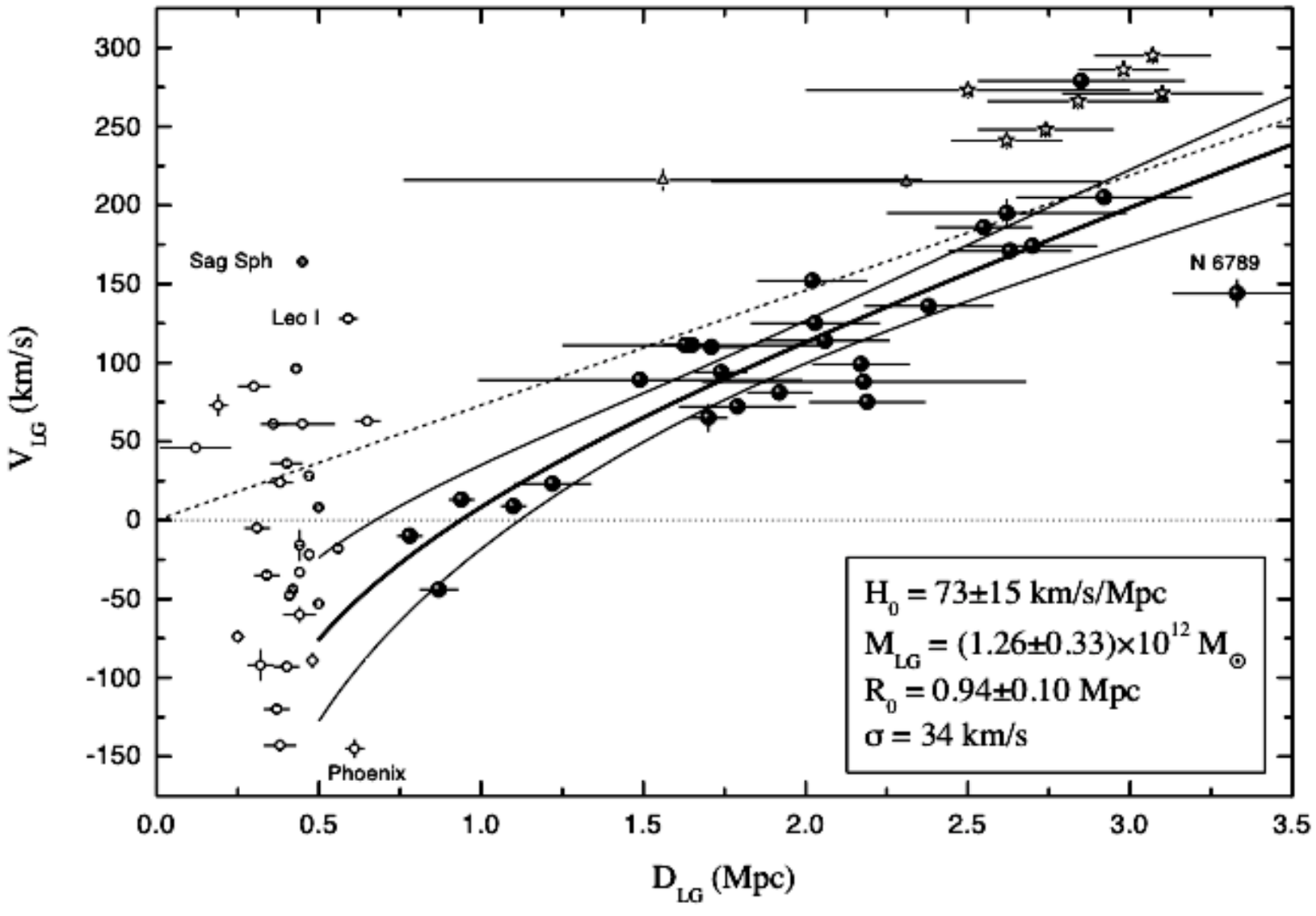

View of the Local Group in supergalactic coordinates

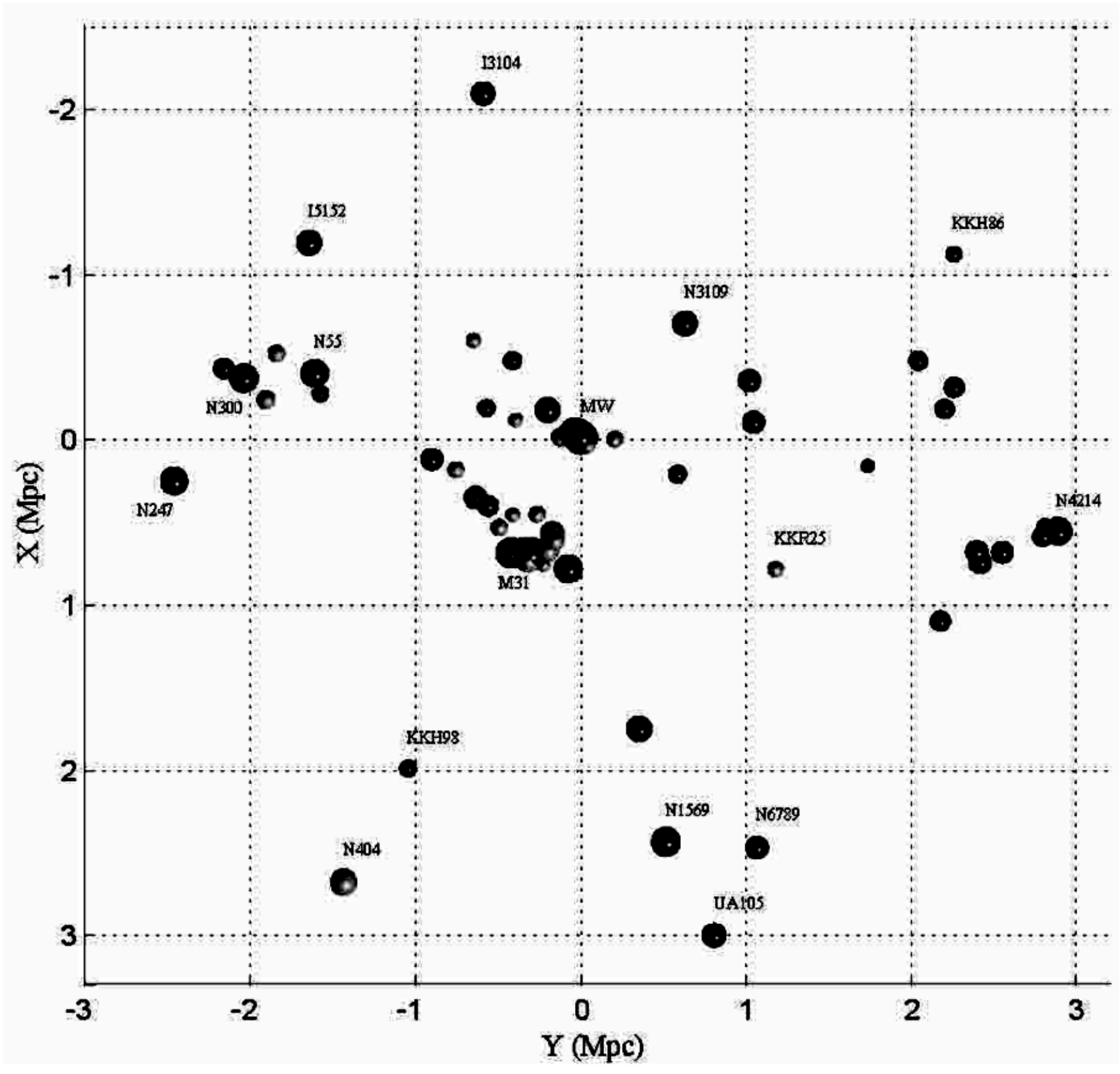

Content of the Local Group: largest galaxies

Name	Morphological type	Abs Mag/circular velocity	Distance
M31	SBb	M	700 kpc
MW	SBb	M	-
M33	Sc	M	600 kpc
M32	dE	M	700 kpc
LMC	Irr	M	50 kpc
NGC6822	Irr	M	500 kpc

NGC6822 dIrr

2Mass JHK image of the central region

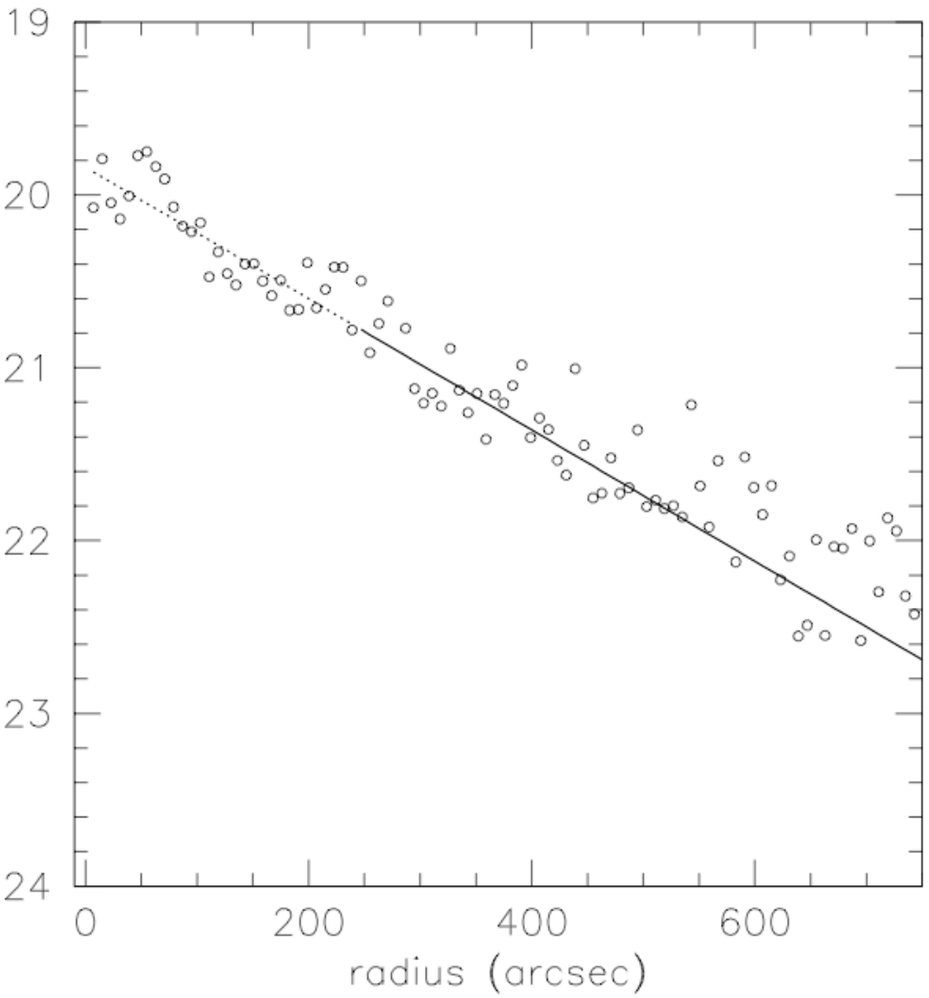

Figure 11. Azimuthally averaged K-band surface brightness profile. The profile is corrected for inclination and Galactic foreground extinction. Spacing between the points is $8''$. The line indicates the exponential disk fit used at radii $R > 240''$.

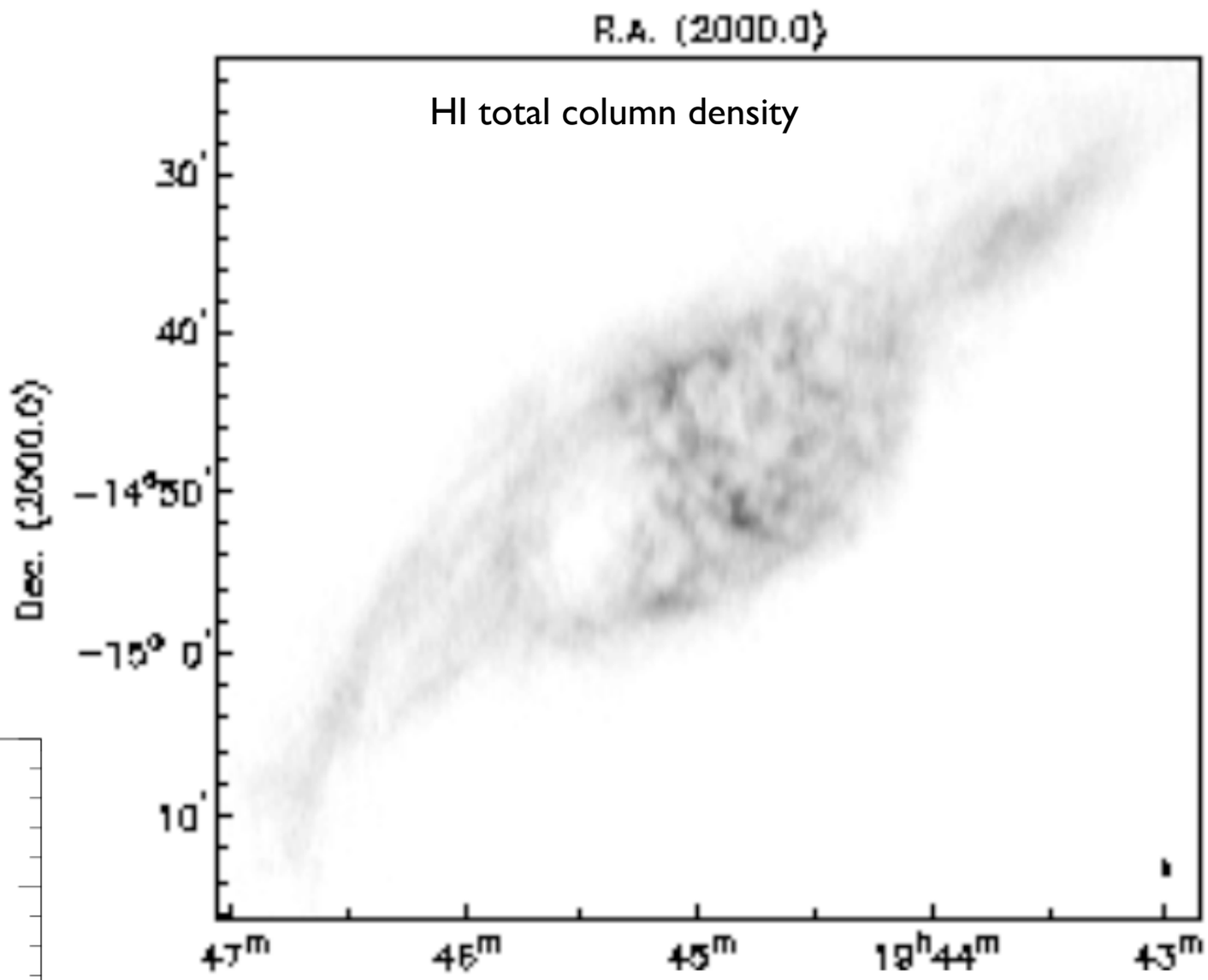

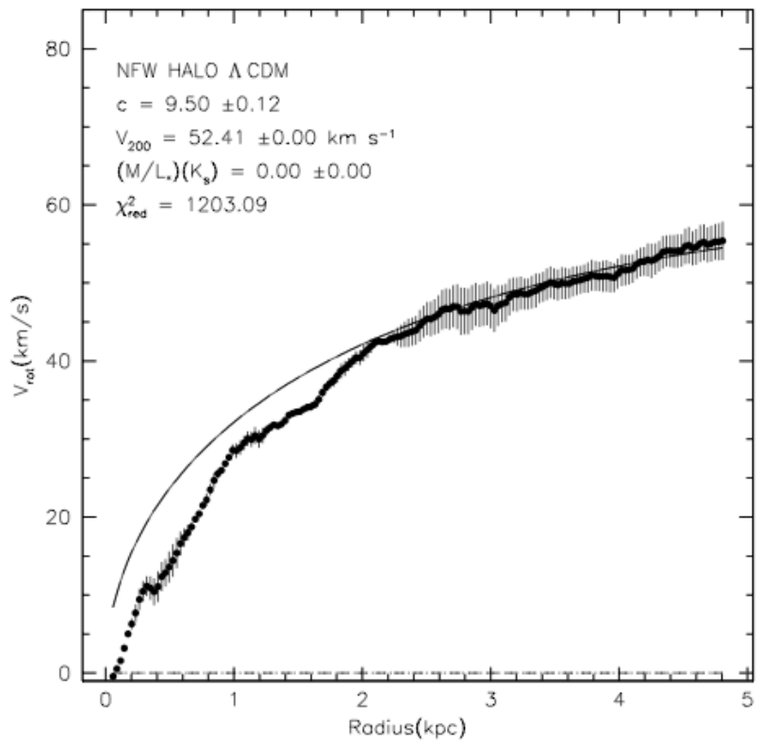

Fornax Dwarf spheroidal

40x40 arcmin B band image

NGC 185 dE galaxy

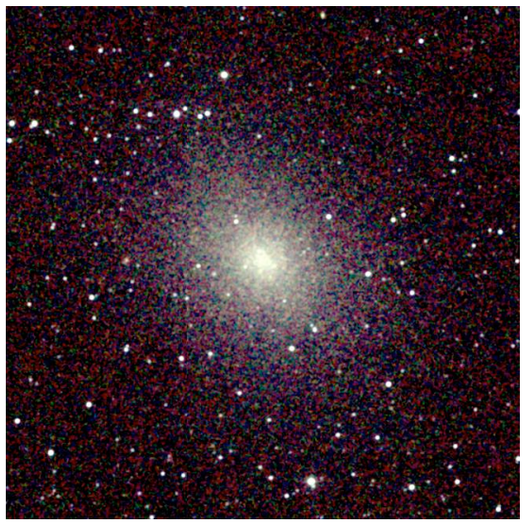

11x11 arcmin 2Mass JHK image

M32 dE galaxy

8x8 arcmin 2Mass JHK image

Morphological types

Normal spirals (S): MW, M31, M33

Dwarf irregular galaxies (dIrrs): gas-rich galaxies with some star formation. They exhibit rotation. Most of them have bars. Examples: LMC, NGC3109, NGC 6822. These are low surface-brightness galaxies with $\mu_V < 23$ mag arcsec^{-2}. Stellar populations range from very old stars to relatively young.

Dwarf elliptical galaxies (dE): M32, NGC 185, NGC 205. Normal elliptical with very high central surface brightness. No rotation, no gas. Old stellar population

Dwarf spheroidal galaxies (dSph): No rotation, no gas. Old stellar population. Low surface brightness $\mu_V > 22$ mag arcsec^{-2} Examples: Fornax, Ursa Minor

Morphological segregation in the number distribution N of different types of galaxies in the Local Group (solid histograms) and in the M81 and Centaurus A groups (hashed histograms) as a function of distance D to the closest massive primary

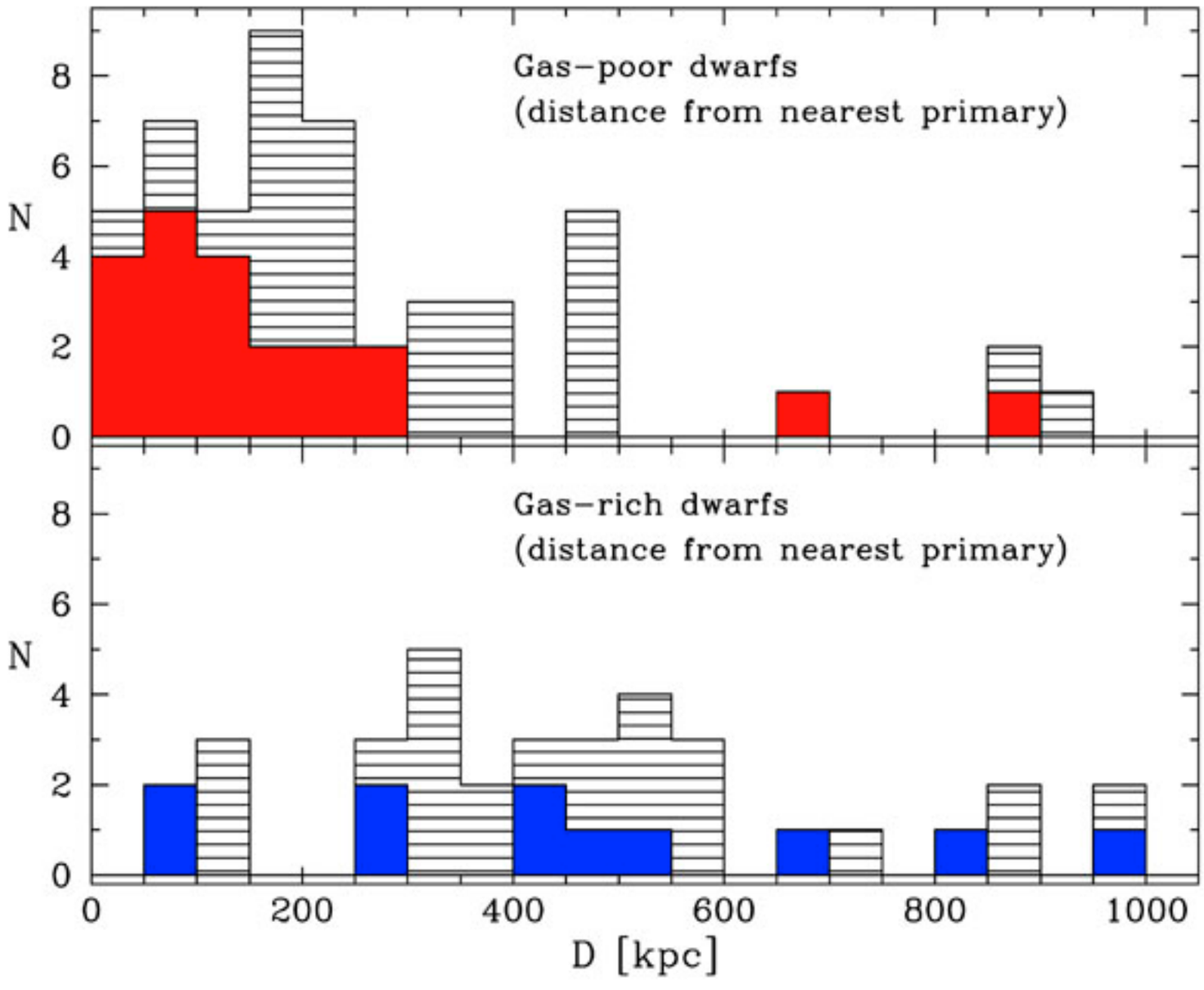

The Metallicity-Luminosity Relation

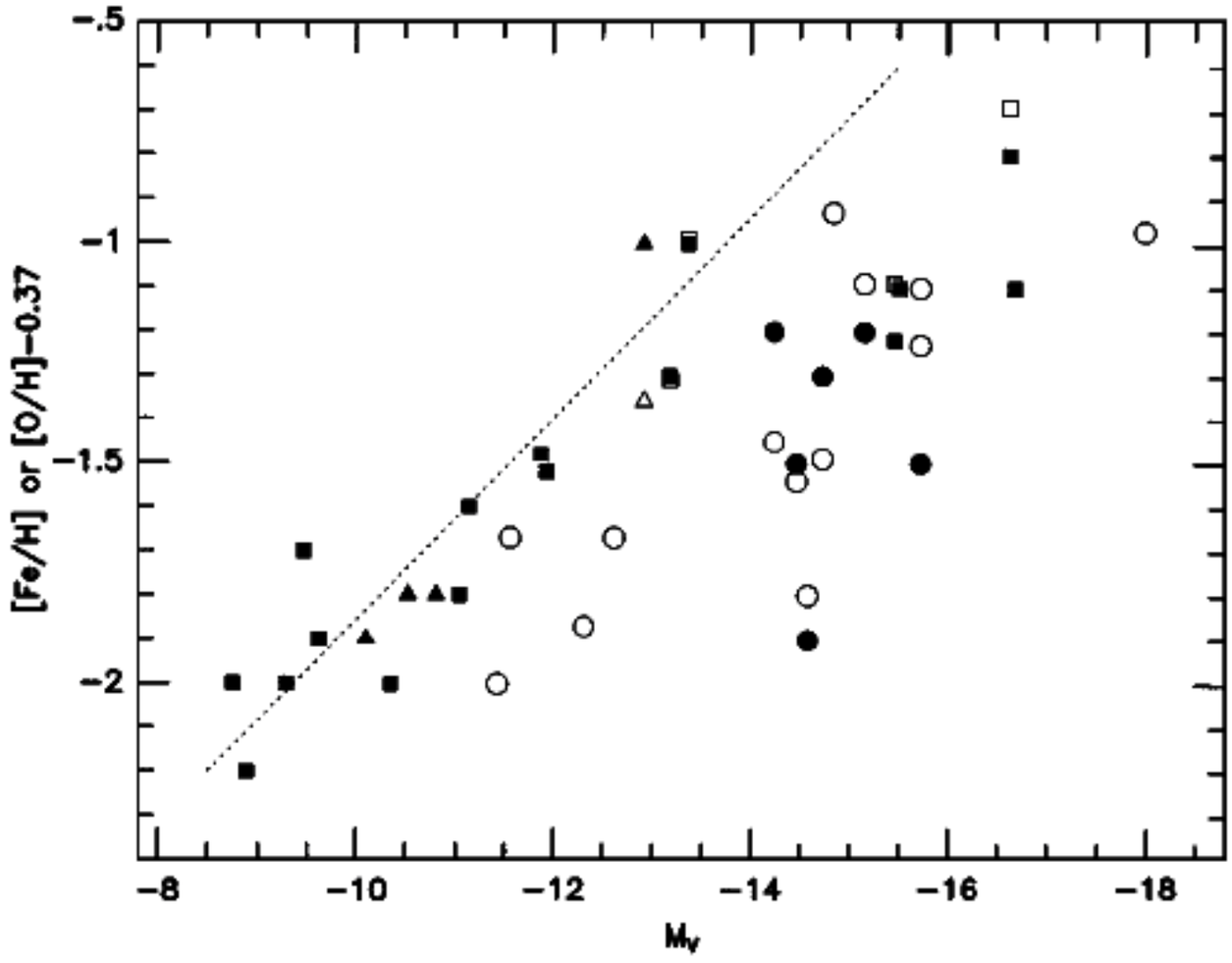

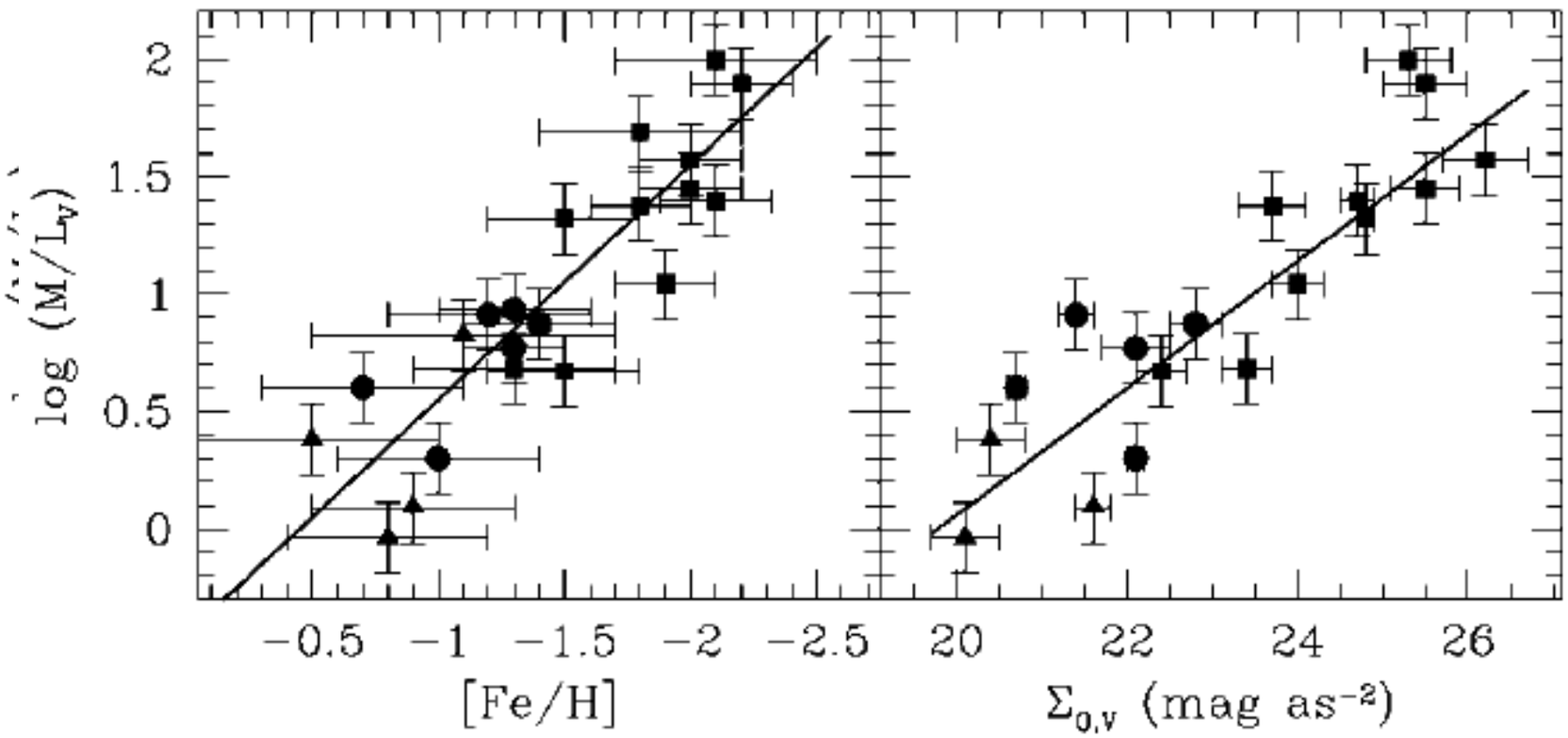

Relation between the mass-to-light ratio (*M*/*L*) and the mean *V* metallicity for our sample of Local Group satellites. Filled squares are the dSph and transition objects (dSph/dIrr); filled circles are the S, Irr, and dIrr satellites; and filled triangles are the dE satellites. The solid line represents a single linear law. *Right*: *M*/*L* ratio vs. the *V*-band central surface brightness *V* for the same galaxies. The solid line is a fit to the data. Prada, Burkert, ApJ, 2002, 564, L73

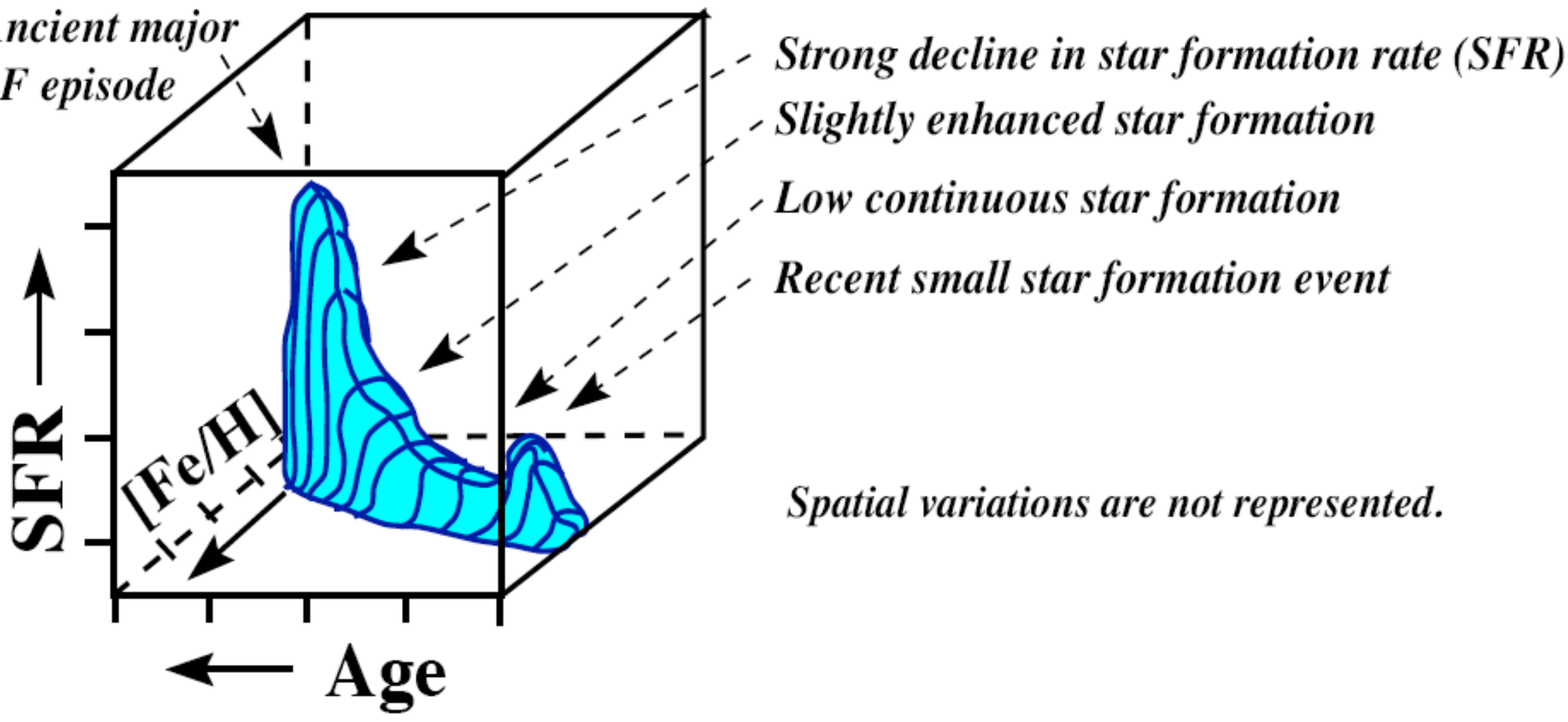

Figure 4: A sample population box for a fictitious galaxy.

E. Grebel 1998

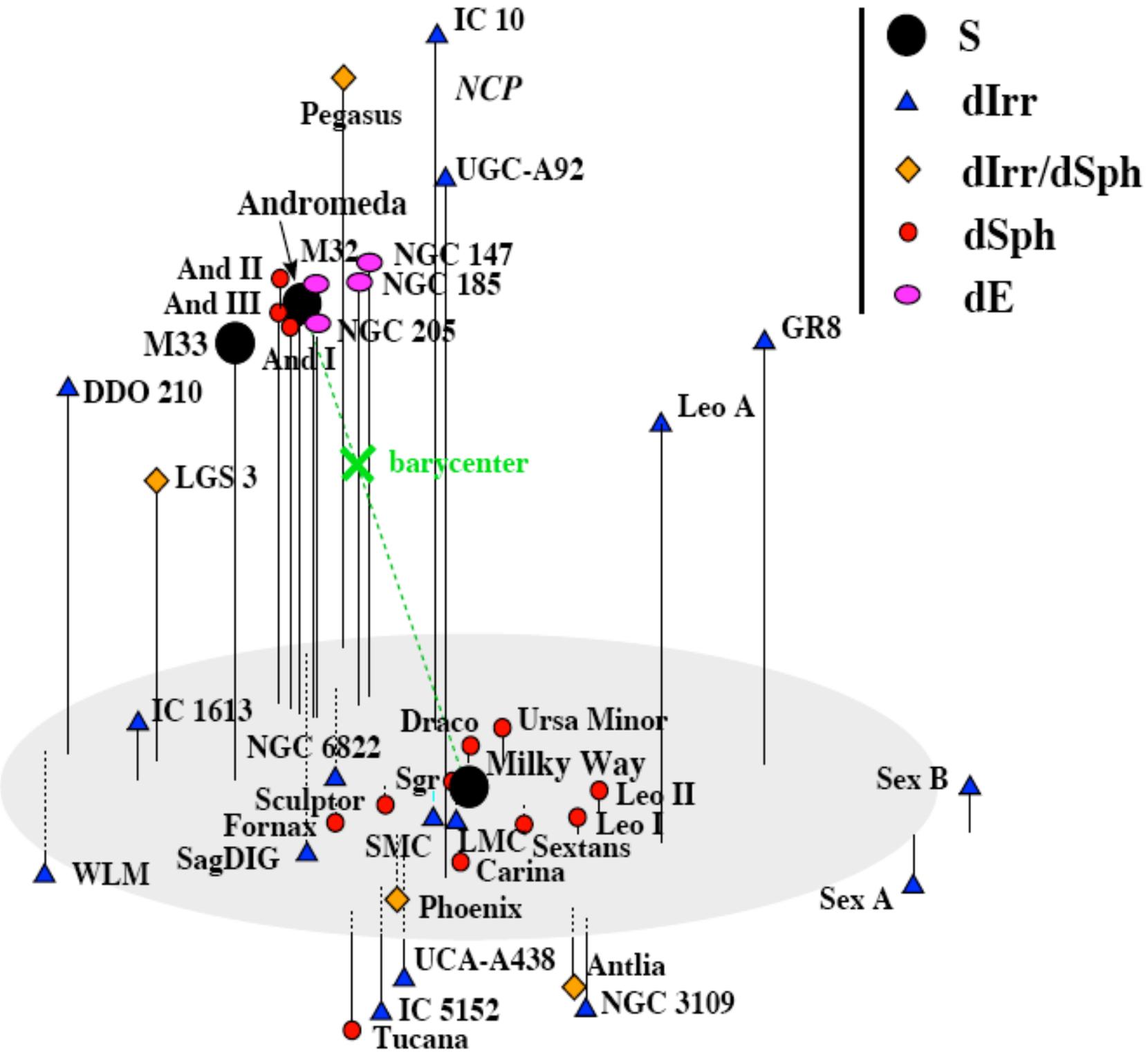
IC 10
NCP
Pegasus
UGC-A92
Andromeda
M32
NGC 147
And II
NGC 185
And III
NGC 205
M33
And I
DDO 210
LGS 3
barycenter
GR8
Leo A
IC 1613
Draco
Ursa Minor
NGC 6822
Milky Way
Sgr
Sculptor
Leo II
Fornax
Leo I
SMC
LMC
Sextans
SagDIG
Carina
WLM
Phoenix
Sex B
Sex A
UCA-A438
Antlia
IC 5152
NGC 3109
Tucana
S
dIrr
dIrr/dSph
dSph
dE

Star Formation Histories of Irregular Galaxies

Grebel 1998

(Distances from barycenter of Local Group) *OB ass. = OB associations, YSG= yellow supergiants, TRGB= tip of the red giant branch, HII = HII regions, WR= W-R stars, Cep= Cepheids, BL= blue loop stars*

[Fe/H]
SFR
Age

IC 10
430 kpc
starburst
WR
Baade sheet
TRGB
?
?
-1
-2
0
15 10 5 0

LMC
470 kpc
8 GCs
spread
clusters & field
-1
-2
0
15 10 5 0

SMC
470 kpc
1 GC
spread
clusters & field
?
-1
0
15 10 5 0

IC 1613
430 kpc
HII
WR
const
RR
C,AGB,YSG
?
-1
0
15 10 5 0

LGS 3
420 kpc
enrich. uncertain
RR
C,AGB
MS
?
-1
-2
0
15 10 5 0 [Gyr]

WLM
770 kpc
1 GC
const
RR,RGB
HII
MS
C,AGB
Cep
-1
-2
0
15 10 5 0

Phoenix
590 kpc
spread
RGB
HII
MS
C
Cep
-1
-2
0
15 10 5 0

Pegasus
440 kpc
spread
RGB
RC
MS
HII
MS
-1
0
15 10 5 0

NGC 6822
650 kpc
~2 GCs
spread
RGB
AGB
OB ass.
WR
-1
-2
0
15 10 5 0

Leo A
870 kpc
enrich. uncertain
RGB
RC
HII
BL
MS
?
-1
-2
0
15 10 5 0 [Gyr]

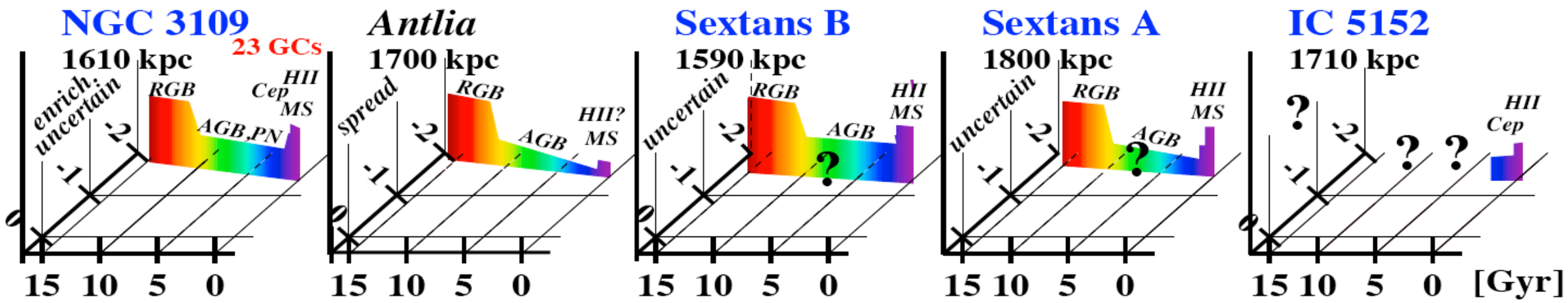

Star Formation Histories of dSph / dE Galaxies

Grebel 1998

MS= main sequence, C = Carbon stars, AGB = asympt. giants, RC= red clump, PN=planetary nebulae, anCep= anomalous Cepheids, RGB = red giant branch, RR = RR Lyrae, HB= horizontal branch

SFR [Fe/H] Age

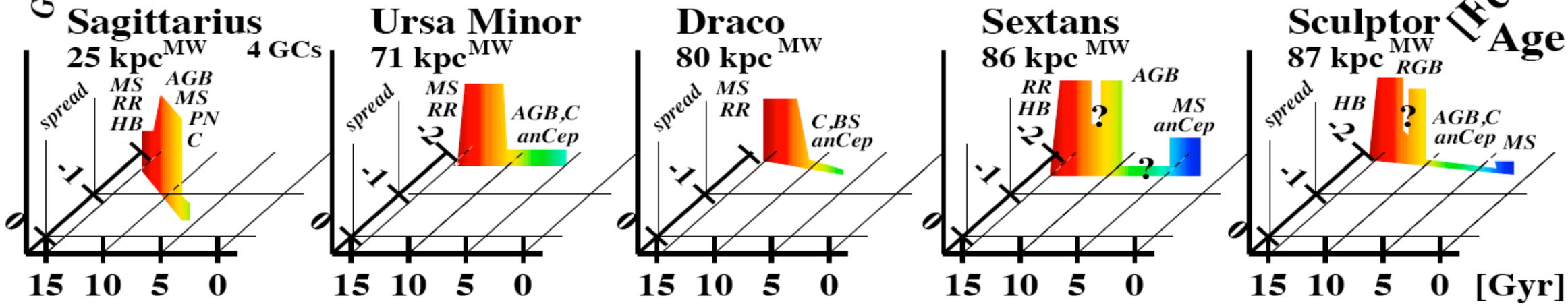

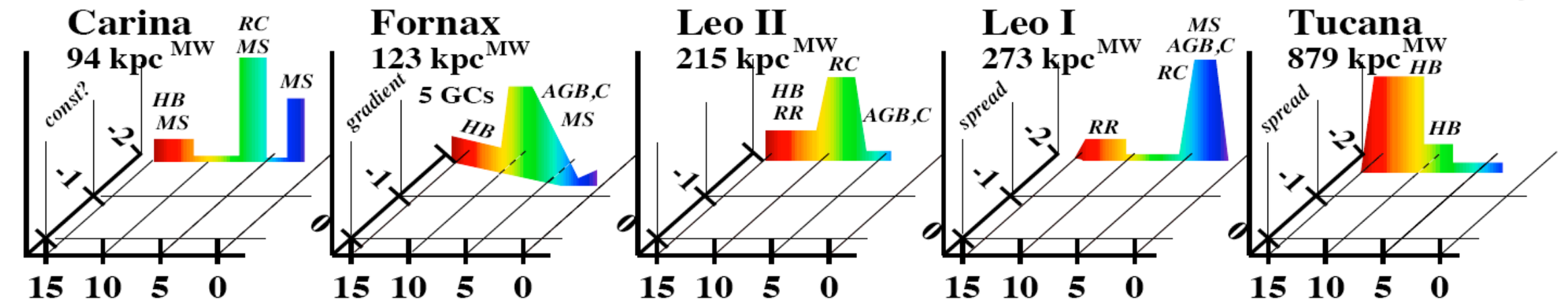

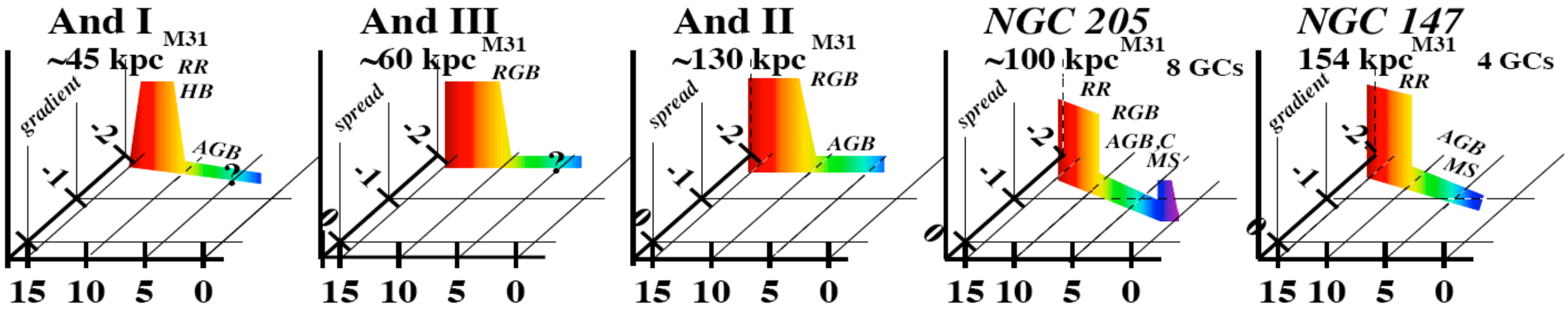
And I
M31
~45 kpc
RR
HB
gradient
AGB
?
-2
-1
0
15 10 5 0
And III
M31
~60 kpc
RGB
spread
?
-2
-1
0
15 10 5 0
And II
M31
~130 kpc
RGB
spread
AGB
-2
-1
0
15 10 5 0
NGC 205
M31
~100 kpc
8 GCs
RR
RGB
AGB,C
MS
spread
-2
-1
0
15 10 5 0
NGC 147
M31
154 kpc
4 GCs
RR
AGB
MS
gradient
-2
-1
0
15 10 5 0

(Left) Known satellite galaxies of the Milky Way within 100 kpc. (Right) LCDM simulation of a Milky Way size halo (Diemand et al. 2008; spanning 800 kpc). The red-shaded cones represent the volume that is currently complete for discovery and characterization of ultra- faint dwarf galaxies. Bullock et al 2010

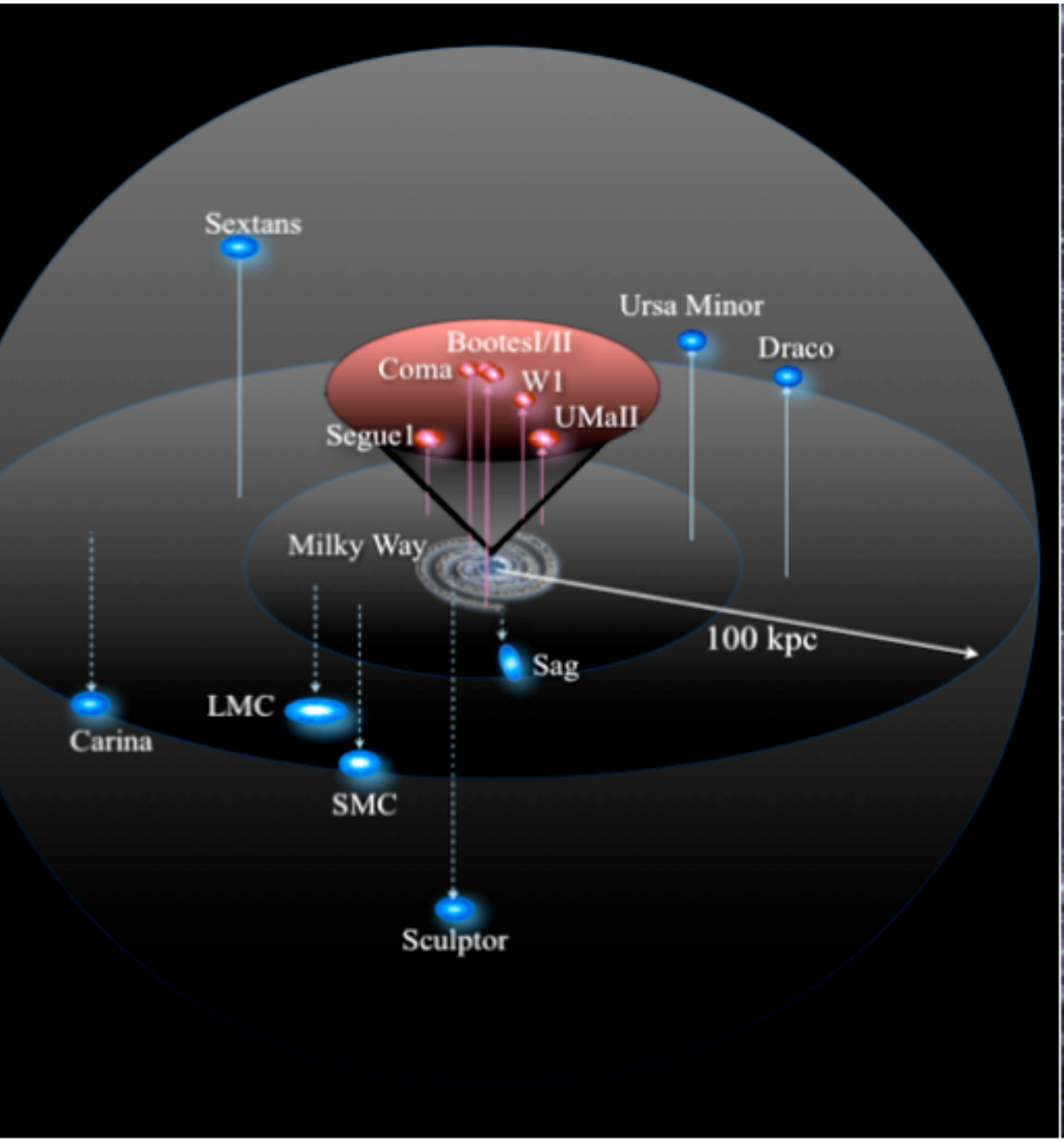

The radius out to which detection is complete for faint dwarf galaxies in various surveys (Tollerud et al. 2008). Known dwarfs are indicated as red circles, which trace the completeness threshold for SDSS.

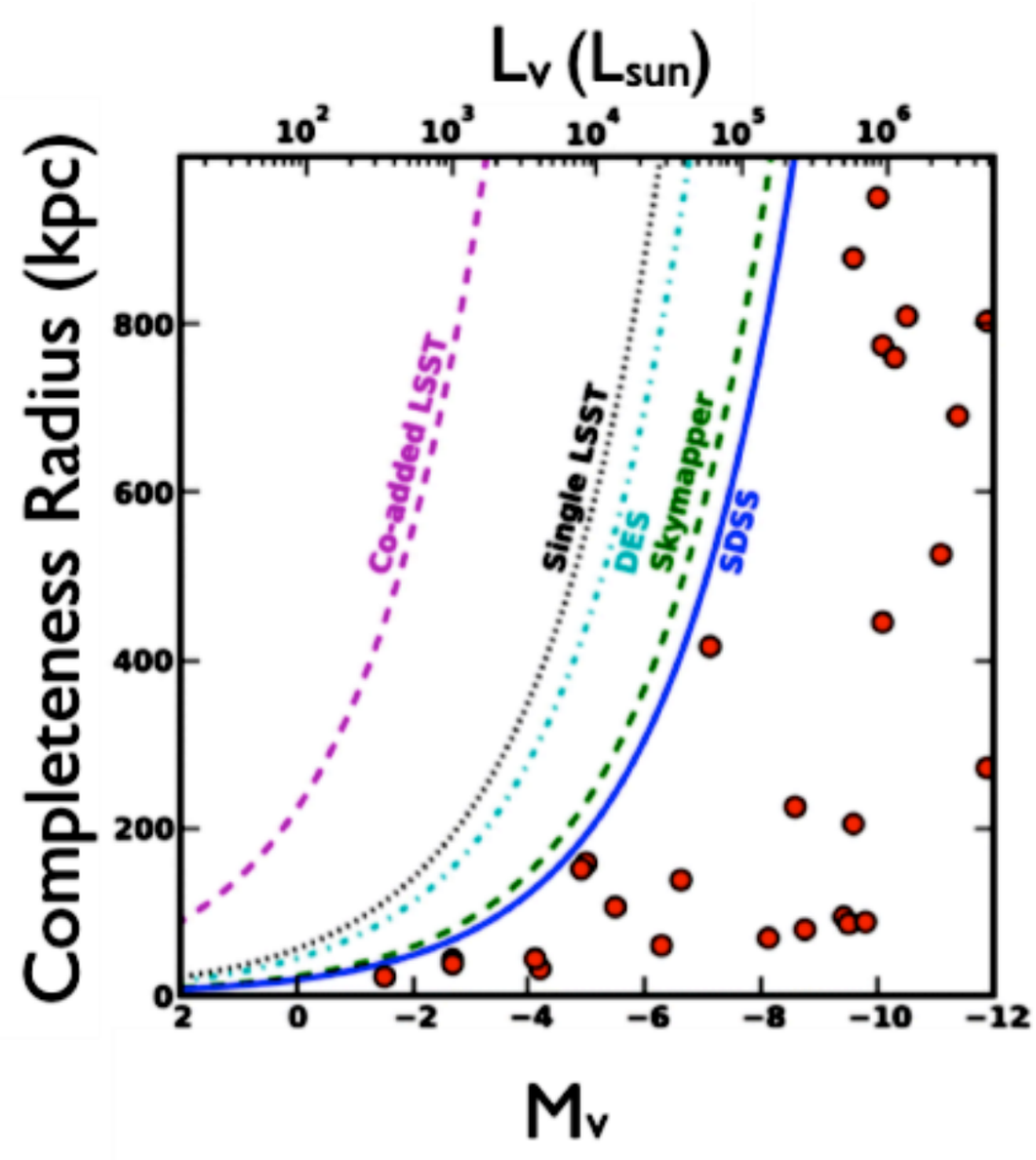

Luminosity functions of Milky Way satellite galaxies within 280 kpc (virial radius) inferred under the assumption of two different radial distributions of satellites, NFW-like (solid black line) and isothermal (dashed black line). The calculation uses the satellite list and the volume correction factor obtained with the pipeline using the cuts r < 22.5. Koposov et al 2008

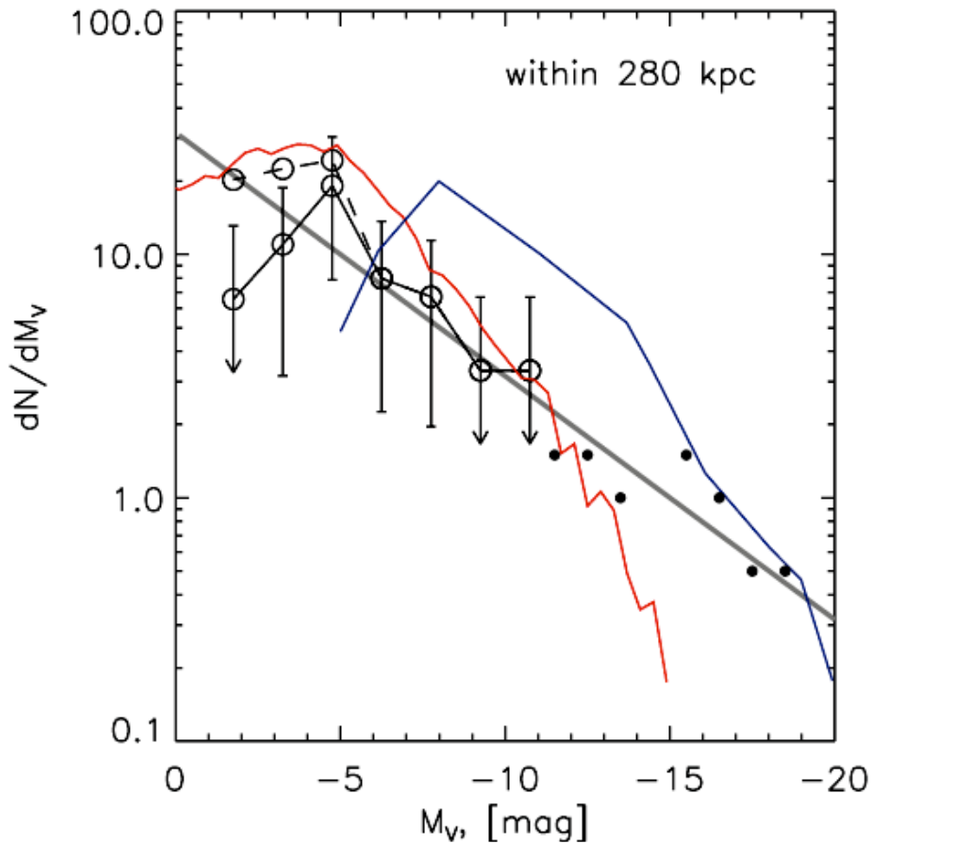

FIG. 14.—Luminosity functions of Milky Way satellite galaxies within ~280 kpc (virial radius) inferred from our analysis under the assumption of two different radial distributions of satellites, NFW-like (*solid black line*) and isothermal (*dashed black line*). The calculation uses the satellite list and the volume correction factor obtained with the pipeline using the cuts $r < 22.5$ and $S_{star} > 5.95$. The arrows on error bars indicate that there is only one galaxy in that particular bin, and so the Poisson error is formally 100%. The theoretical prediction of Fig. 1 of Benson et al. (2002) is shown as a red line, and the prediction of Somerville (2002) for $z_{reion} = 10$ is shown as a blue line. In addition, the luminosity function for the bright ($M_V < -11$) satellites of the Milky Way sampled over the whole sky together with the bright M31 satellites within 280 kpc from Metz et al. (2007) is plotted with small filled circles (the list of plotted objects consists of Sgr, LMC, SMC, Scl, For, Leo II, Leo I, M32, NGC 205, And I, NGC 147, And II, NGC 185, And VII, and IC 10). The function $dN/dM_V = 10 \times 10^{0.1(M_V+5)}$ is shown in gray.

Luminosity function as observed (lower curve), corrected only for SDSS sky coverage (middle curve), and with all corrections included (upper curve). Note that the classical (pre-SDSS) satellites are uncorrected, while new satellites have the correction applied. Tollerud et al 2008

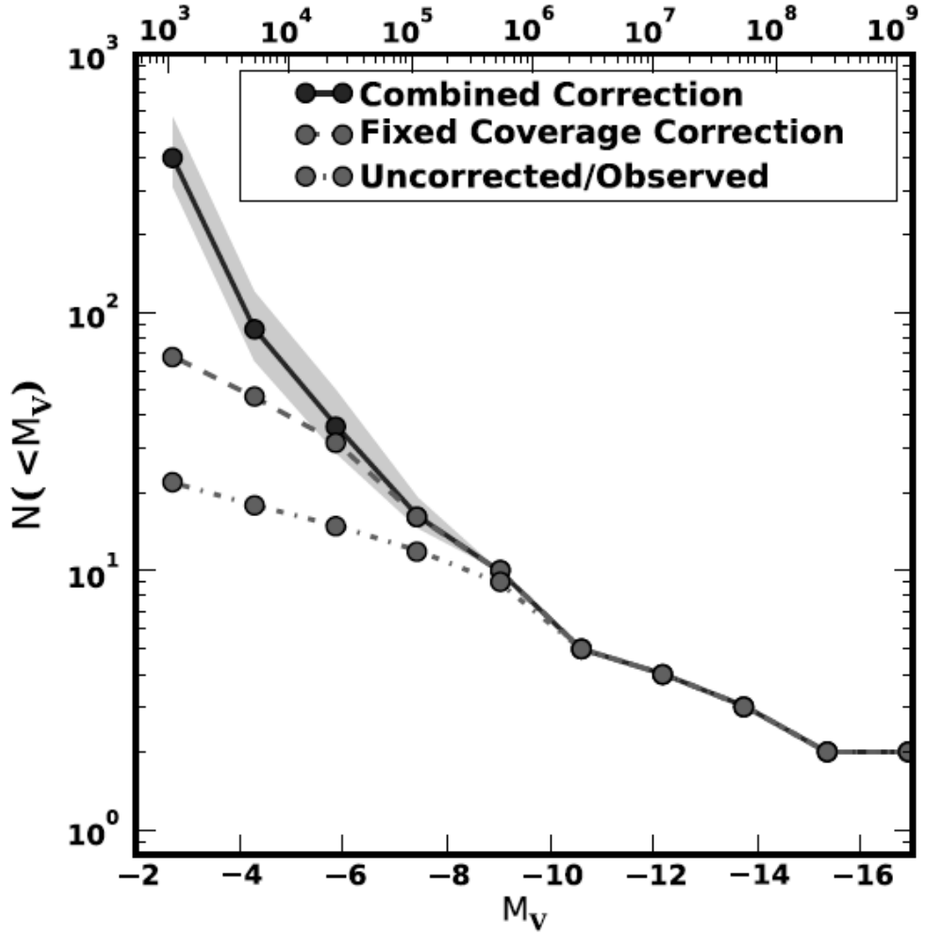

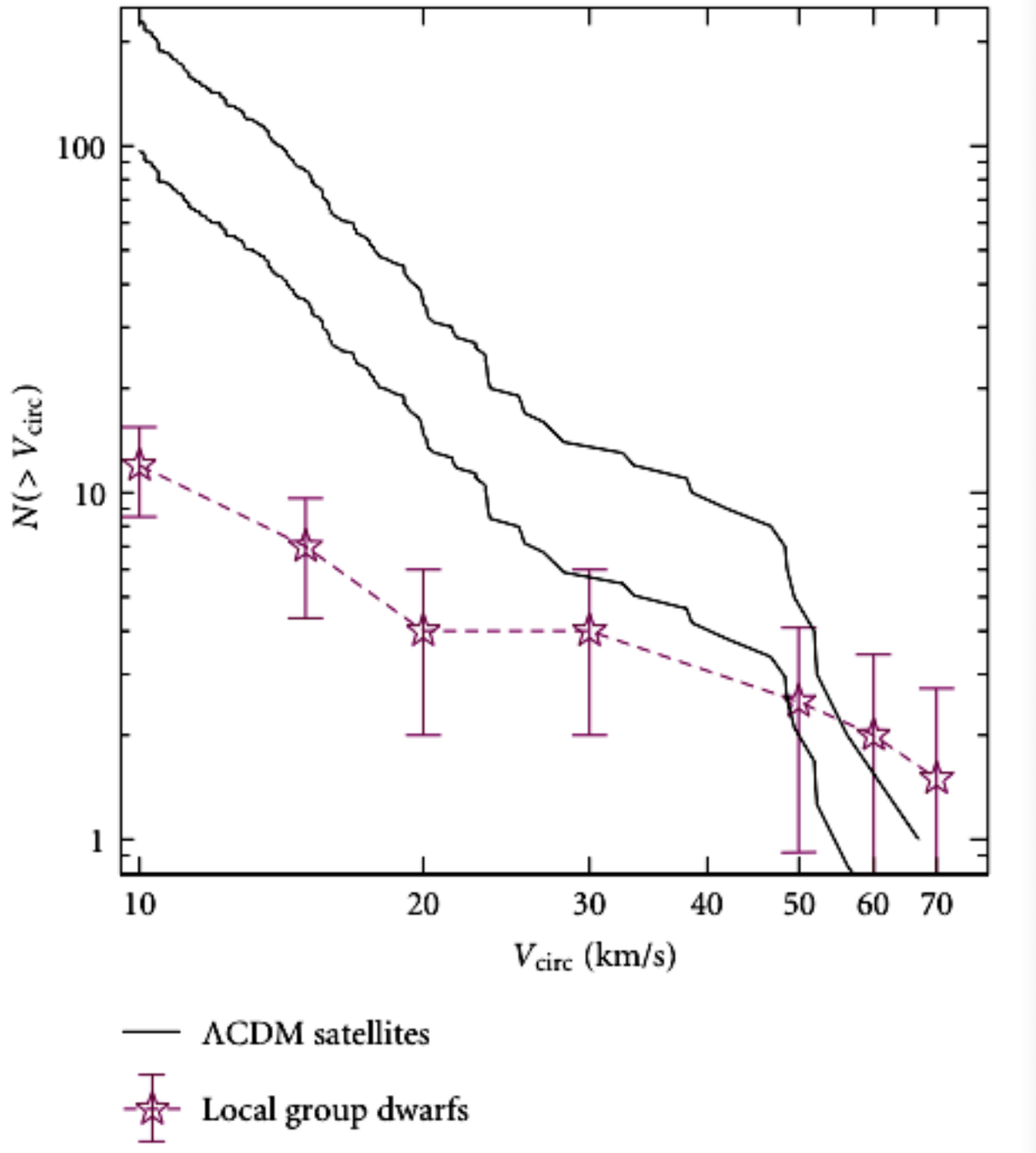

FIGURE 7: Comparison of the cumulative circular velocity functions, $N(> V_{\rm max})$, of subhalos and dwarf satellites of the Milky Way within the radius of 286 kpc (this radius is chosen to match the maximum distance to observed satellites in the sample and is smaller than the virial radius of the simulated halo, $R_{337} = 326$ kpc). The subhalo VFs are plotted for the host halos with maximum circular velocities of 160 km/s and 208 km/s that should bracket the $V_{\rm max}$ of the actual Milky Way halo. The VF for the observed satellites was constructed using circular velocities estimated from the line-of-sight velocity dispersions as $V_{\rm max} = \sqrt{3}\sigma_r$ (see the discussion in the text for the uncertainties of this conversion).

Structure of Dwarf Spheroidals

Projected velocity dispersion profiles for six Milky Way dSph satelli
Overplotted are profiles corresponding to mass-follows light (King
1962) models (dashed lines; these fall to zero at the nominal “edge
stellar distribution), and best-fitting NFW profiles that assume cons
velocity anisotropy. Short, vertical lines indicate luminous core radi
Distance moduli are adopted from Mateo (1998)

Walker et al 20(

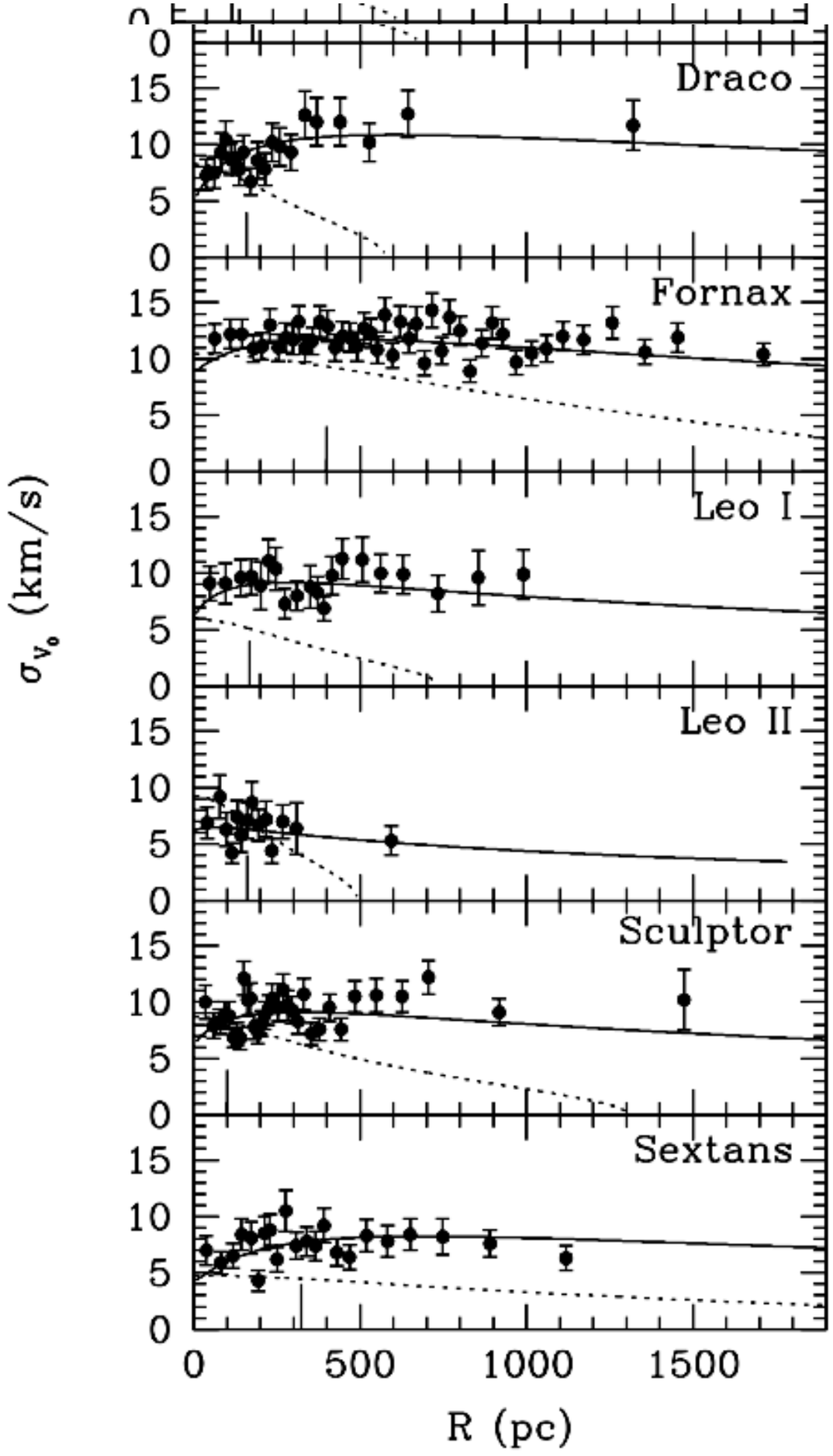

Solid lines represent density, mass and M/L profiles corresponding to best-fitting NFW profiles.

Dotted lines in the top and middle panels are baryonic density and mass profiles, respectively, following from the assumption that the stellar component (assumed to have M/L=1) has exponentially falling density

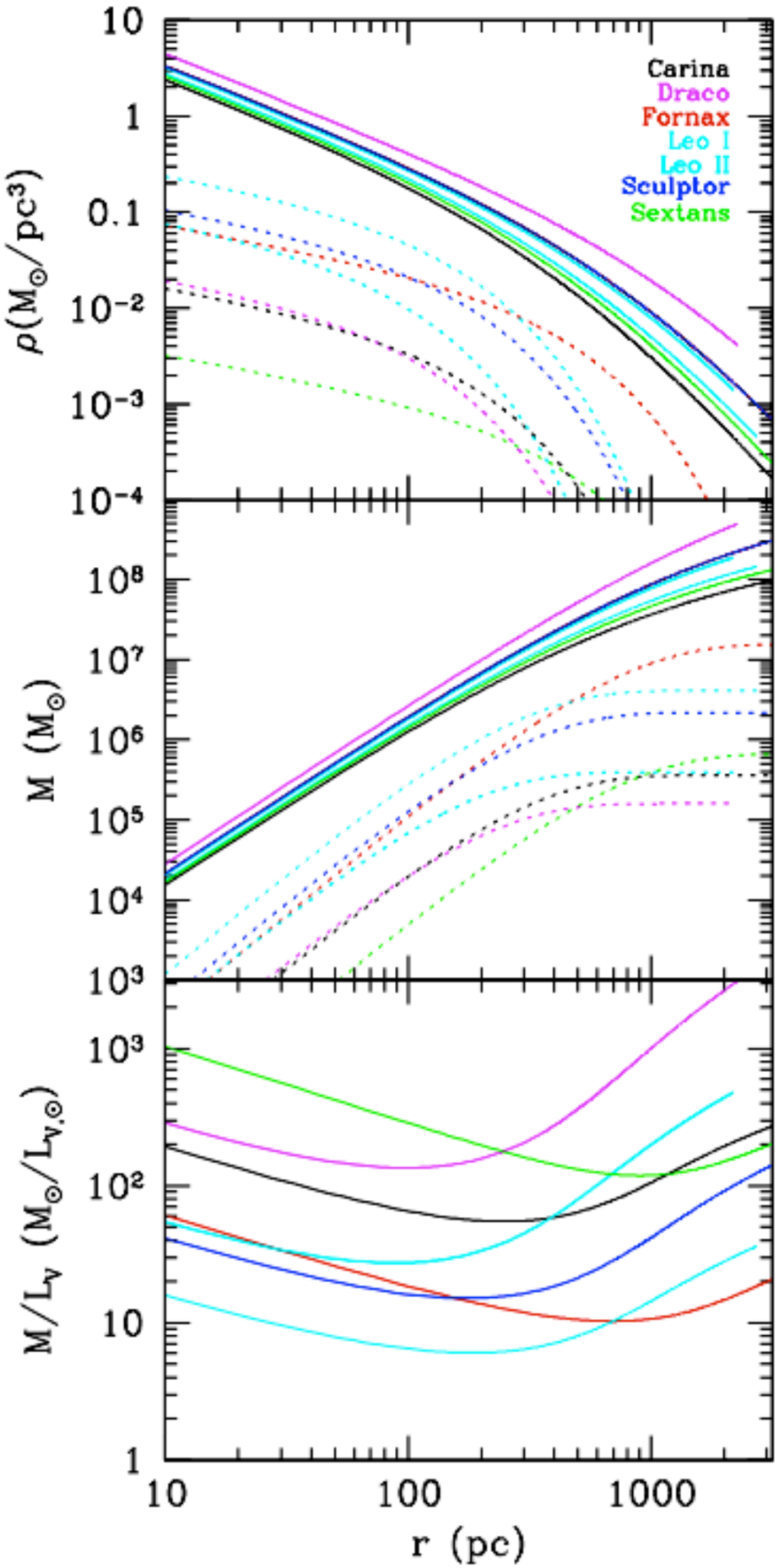

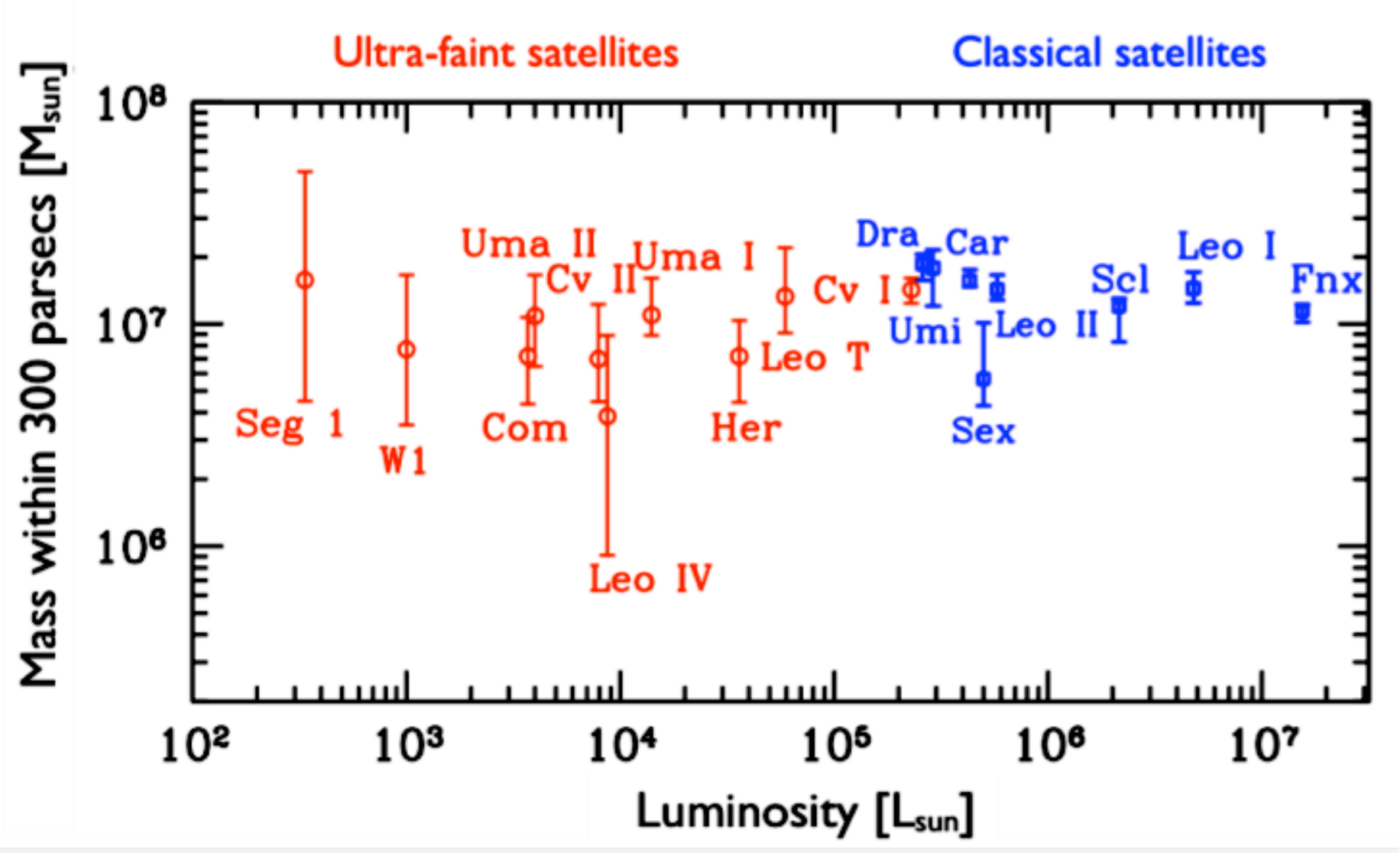

The integrated mass within the inner 300pc of Milky Way satellite galaxies as a function of their luminosities (Strigari et al. 2008). Satellites discovered since 2004 are shown in red.

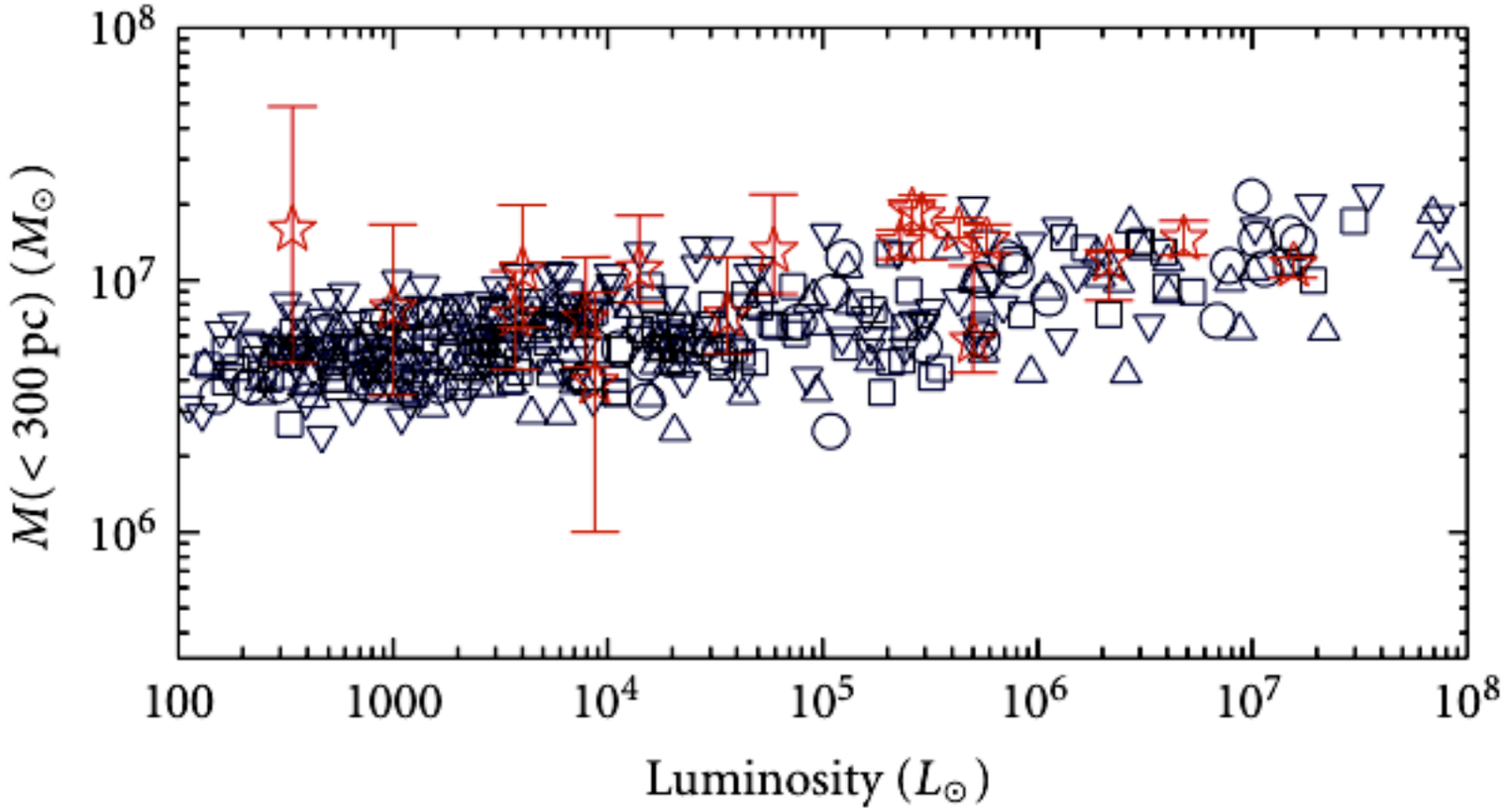

FIGURE 10: The mass within the central 300 pc versus luminosity for the dwarf satellites of the Milky Way (stars with error bars, see [88]). The open symbols of different types show the expected relation for subhalos in three different Milky Way-sized halos formed in the simulations of the concordance ΛCDM cosmology if the luminosity of the subhalos is related to their virial mass at accretion epoch as $L = 5 \times 10^3 L_\odot (M_{\mathrm{vir,acc}}/10^9 M_\odot)^{2.5}$ (see text for discussion).

Kravtsov 2009

Accurate masses for dispersion-supported galaxies,
J.Wolf et al MN, 406,1220, 2010

$$M_{1/2} \equiv M(r_{1/2}) \simeq 3G^{-1}\langle\sigma^2_{\rm los}\rangle\, r_{1/2},$$
$$\simeq 4G^{-1}\ \langle\sigma^2_{\rm los}\rangle R_{\rm e}\,,$$
$$\simeq 930\left(\frac{\langle\sigma^2_{\rm los}\rangle}{\rm km^2\,s^{-2}}\right)\left(\frac{R_{\rm e}}{\rm pc}\right)\ {\rm M}_\odot\,.$$

In the second line, we have used $R_{\rm e} \simeq (3/4)\,r_{1/2}$ for the two-dimensional (2D) projected half-light radius. This approximation is accurate to better than 2 per cent for exponential, Gaussian, King, Plummer and Sérsic profiles (see Appendix B for useful fitting formulae).

$$-n_\star\frac{{\rm d}\Phi}{{\rm d}r} = \frac{{\rm d}(n_\star\sigma_{\rm r}^2)}{{\rm d}r} + 2\frac{\beta\, n_\star\sigma_{\rm r}^2}{r}.$$

Here $\sigma_{\rm r}(r)$ is the radial velocity dispersion of the stars/tracers and $\beta(r) \equiv 1 - \sigma_{\rm t}^2/\sigma_{\rm r}^2$ is a measure of the velocity anisotropy, where the tangential velocity dispersion $\sigma_{\rm t} = \sigma_\theta = \sigma_\phi$. It is informative to rewrite the implied total mass profile as

$$M(r) = \frac{r\sigma_{\rm r}^2}{G}\,(\gamma_\star + \gamma_\sigma - 2\beta)\,, \qquad (9)$$

where $\gamma_\star \equiv -{\rm d}\ln n_\star/{\rm d}\ln r$ and $\gamma_\sigma \equiv -{\rm d}\ln\sigma_{\rm r}^2/{\rm d}\ln r$. Without the

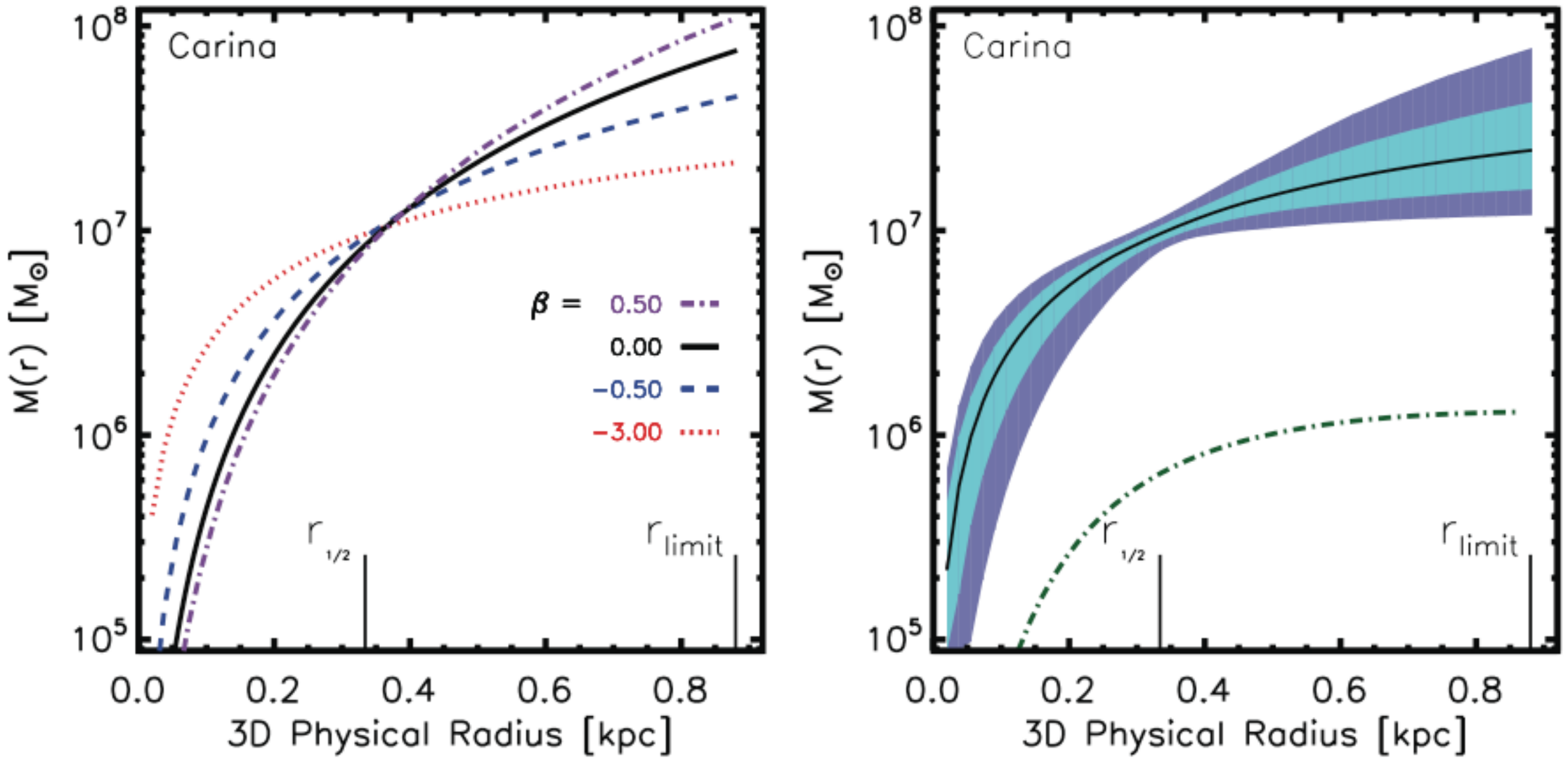

Figure 1. *Left:* the cumulative mass profile generated by analysing the Carina dSph using four different constant velocity dispersion anisotropies. The lines represent the median cumulative mass value from the likelihood as a function of physical radius. The width of the mass likelihoods (not shown) does not vary much with radius and are approximately the size of the width at the pinch in the right-hand panel. *Right:* the cumulative mass profile of the same galaxy, where the black line represents the median mass from our full mass likelihood (which allows for a radially varying anisotropy). The different shades represent the inner two confidence intervals (68 and 95 per cent). The green dot–dashed line represents the contribution of mass from the stars, assuming a stellar *V*-band mass-to-light ratio of $3\,M_{\odot}/L_{\odot}$.

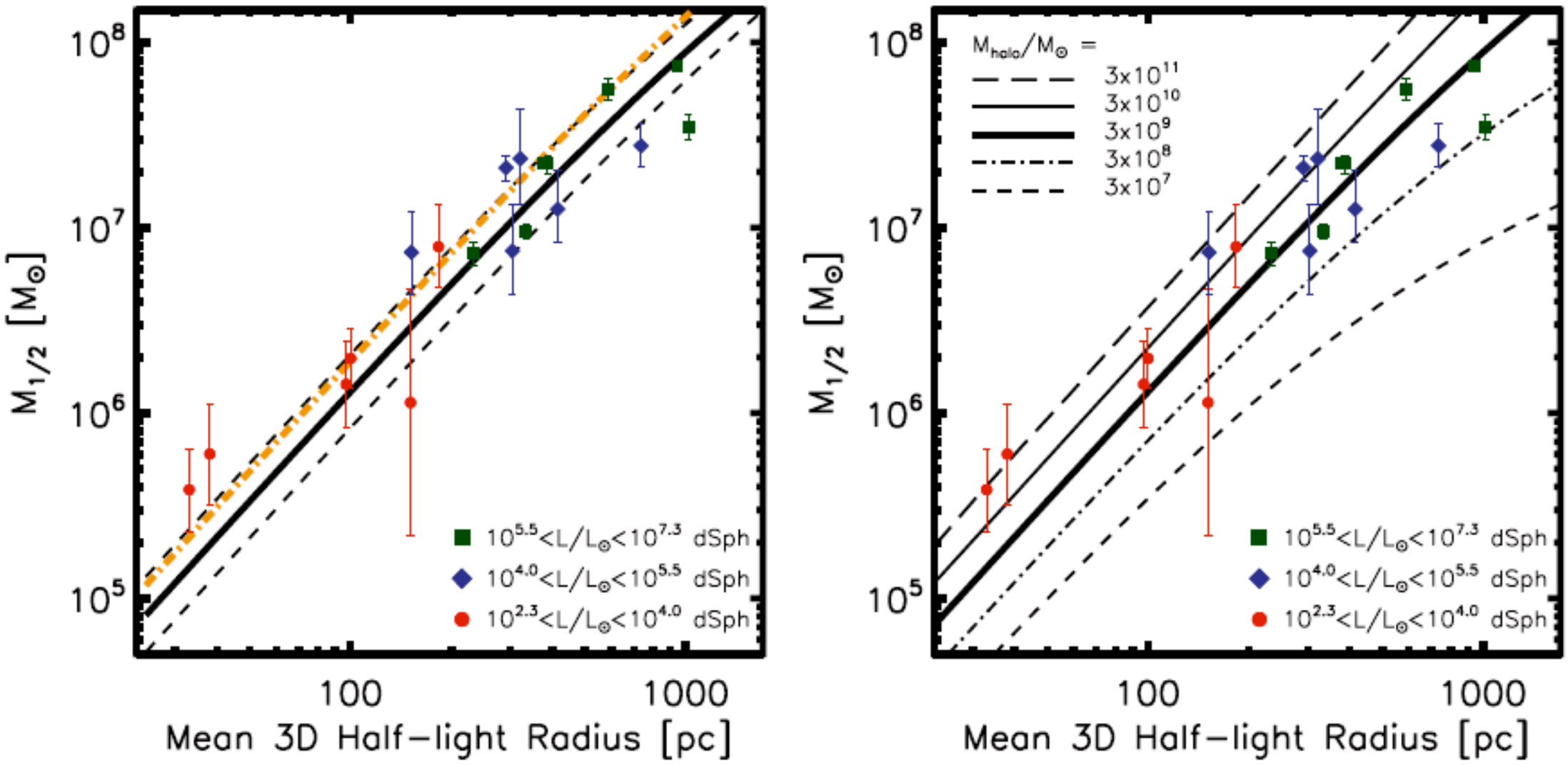

Figure 3. The half-light masses of the MW dSphs plotted against $r_{1/2}$. *Left:* the solid black line shows the NFW mass profile for a field halo of $M_{\rm halo} = 3 \times 10^9\,{\rm M}_\odot$ at $z = 0$ expected for a *WMAP*5 cosmology ($c = 11$ according to Macciò et al. 2008), where the two dashed lines correspond to a spread in concentration of $\Delta \log_{10}(c) = 0.14$, as determined by N-body simulations (Wechsler et al. 2002). The orange dot–dashed line shows the profile for a median $M_{\rm halo} = 3 \times 10^9\,{\rm M}_\odot$ at $z = 3$. *Right:* the same data points along with the (median c) NFW mass profiles for haloes with $M_{\rm halo}$ masses ranging from 3×10^7 to $3 \times 10^{11}\,{\rm M}_\odot$ (from bottom to top). We note that while all but one of the MW dSphs are consistent with sitting within a halo of a common mass (left), many of the dwarfs can also sit in haloes of various masses (right). There is no indication that lower luminosity galaxies (red circles) are associated with less massive haloes than the highest mass galaxies (green squares), as might be expected in simple models of galaxy formation. None of these galaxies are associated with a halo less massive than $M_{\rm halo} \simeq 3 \times 10^8\,{\rm M}_\odot$.

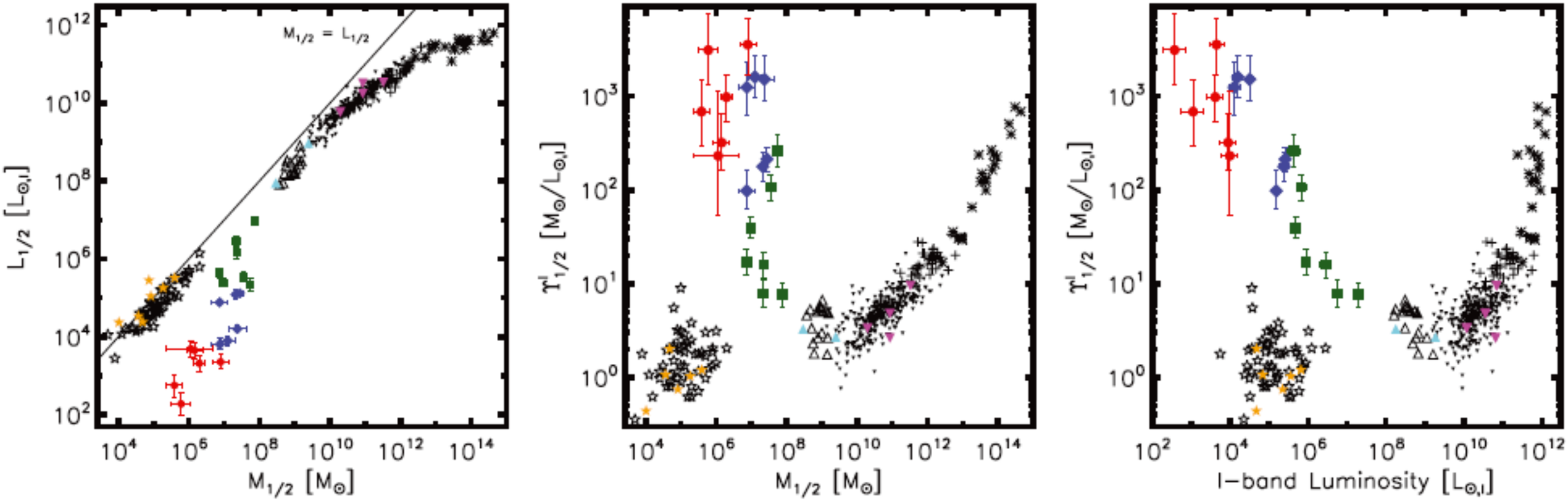

Figure 4. *Left:* the half I-band luminosity $L_{1/2}$ versus half-light mass $M_{1/2}$ for a broad population of spheroidal galaxies. *Middle:* the dynamical I-band half-light mass-to-light ratio $\Upsilon^I_{1/2}$ versus $M_{1/2}$ relation. *Right:* the equivalent $\Upsilon^I_{1/2}$ versus total I-band luminosity $L_I = 2\,L_{1/2}$ relation. The solid line in the left-hand panel guides the eye with $M_{1/2} = L_{1/2}$ in solar units. The solid, coloured points are all derived using our full mass likelihood analysis and their specific symbols/colours are linked to galaxy types as described in Fig. 2. The I-band luminosities for the MW dSph and GC population were determined by adopting M92's $V - I = 0.88$. All open, black points are taken from the literature as follows. Those with $M_{1/2} > 10^8\,\mathrm{M}_\odot$ are modelled using equation (2) with $\sigma_{\rm los}$ and $r_{1/2}$ culled from the compilation of Zaritsky et al. (2006): triangles for dwarf ellipticals (Geha, Guhathakurta & van der Marel 2003), inverse triangles for ellipticals (Jørgensen, Franx & Kjaergaard 1996; Matković & Guzmán 2005), plus signs for brightest cluster galaxies (Oegerle & Hoessel 1991) and asterisks for cluster spheroids, which, following Zaritsky et al. (2006), include the combination of the central brightest cluster galaxy and the extended intracluster light. Stars indicate globular clusters, with the subset of open, black stars taken from Pryor & Meylan (1993).

Wolf et al 2010

We show that dissipationless ΛCDM simulations predict that the majority of the most massive subhalos of the Milky Way are too dense to host any of its bright satellites ($L_V > 105 L_\odot$). These dark subhalos have circular velocities at infall of Vinfall = 30 –70 km s^{-1} and infall masses of [0.2 –4] $\times 10^{10} M_\odot$.

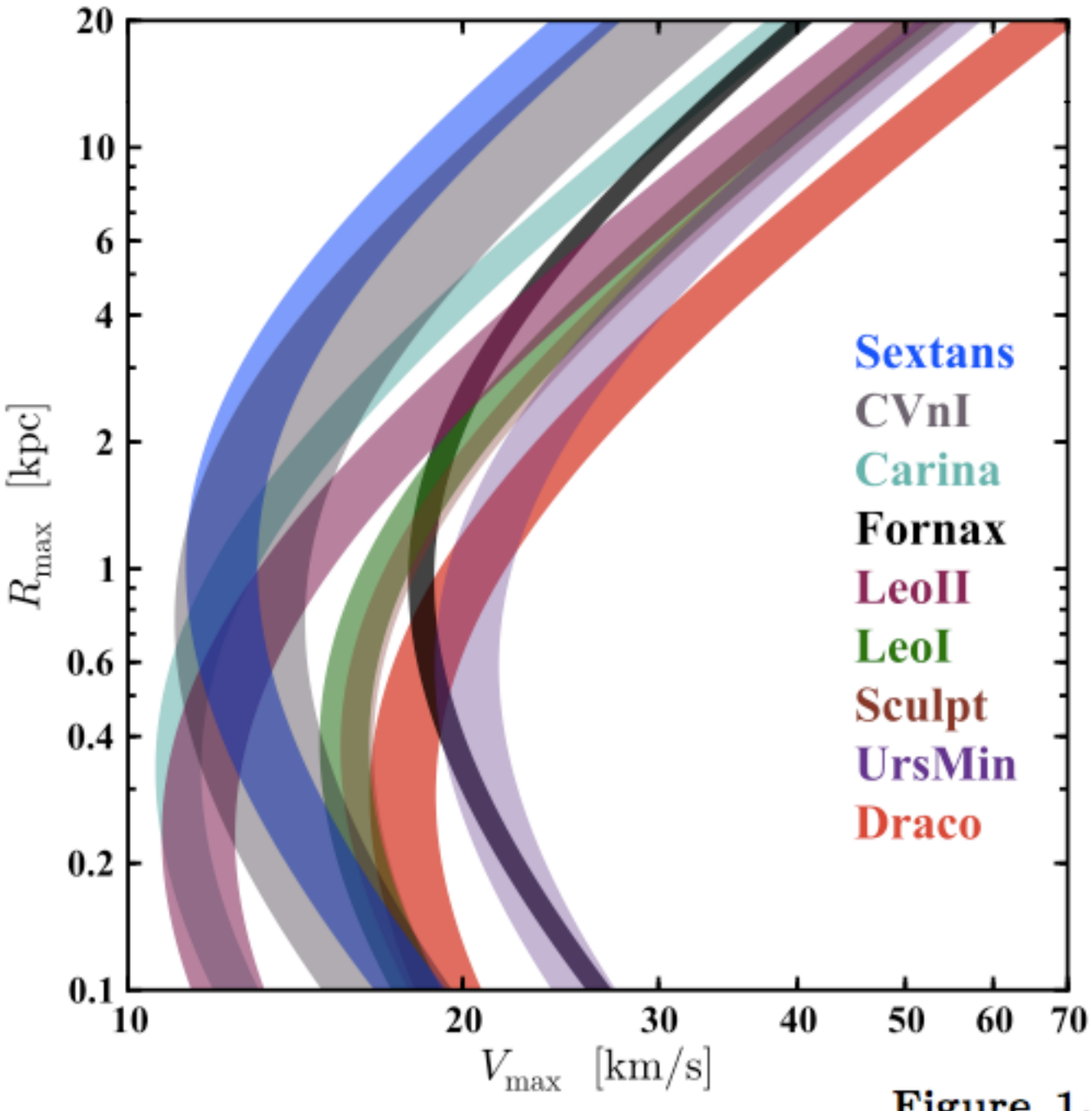

Figure 1. Constraints on the $V_{\rm max} - R_{\rm max}$ values (assuming NFW profiles) of the hosts of the nine bright ($L_V > 10^5\, L_\odot$) MW dwarf spheroidal galaxies. The colored bands show $1\,\sigma$ confidence intervals based on measured values of $R_{1/2}$ and $M_{1/2}$ from Wolf et al. (2010).

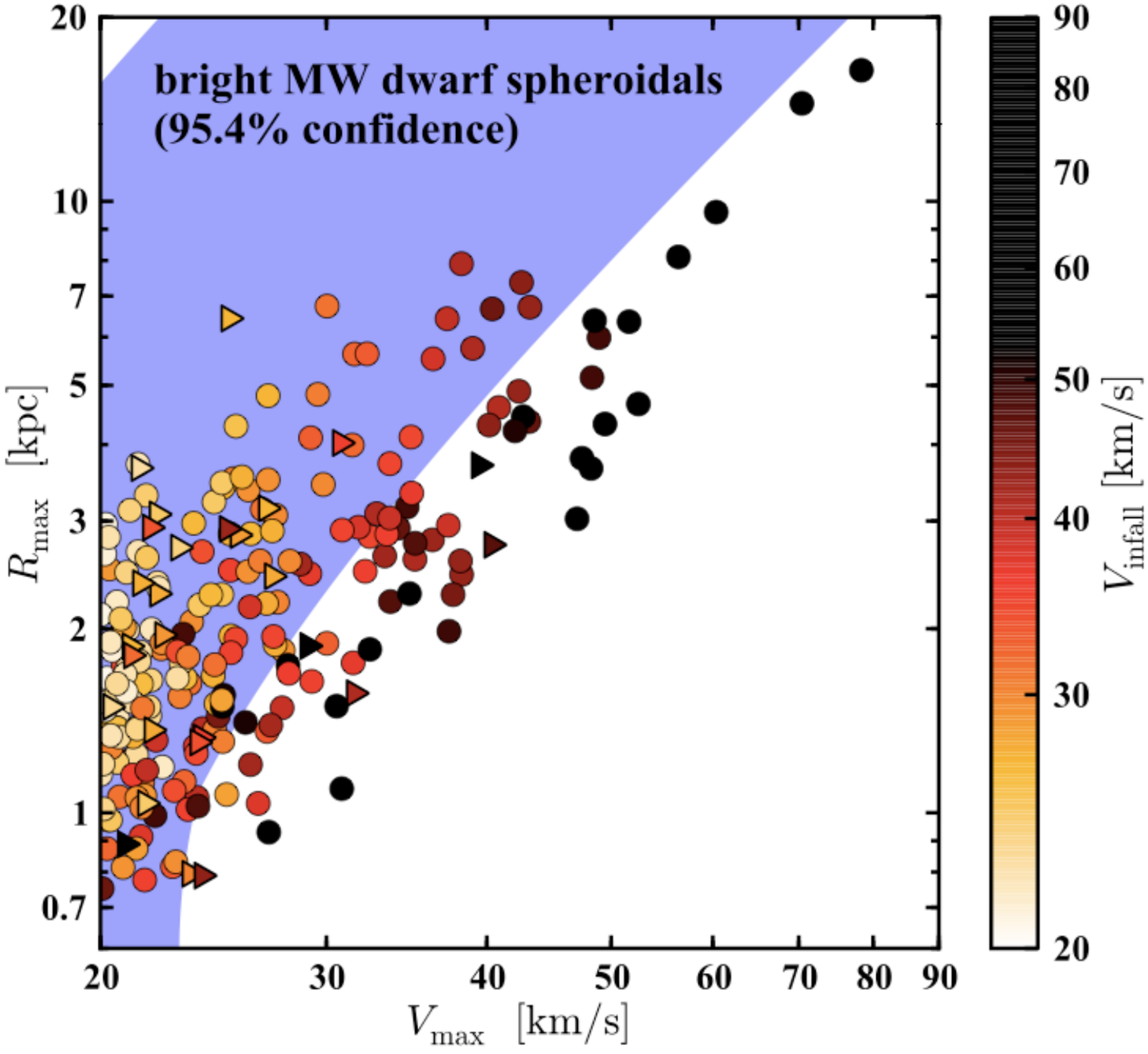
bright MW dwarf spheroidals
(95.4% confidence)
20
10
7
5
3
2
1
0.7
$R_{\rm max}$ [kpc]
20
30
40
50
60
70
80
90
$V_{\rm max}$ [km/s]
90
80
70
60
50
40
30
20
$V_{\rm infall}$ [km/s]

M. Boylan-Kolchin, J. S. Bullock, and M. Kaplinghat ApJ 2012

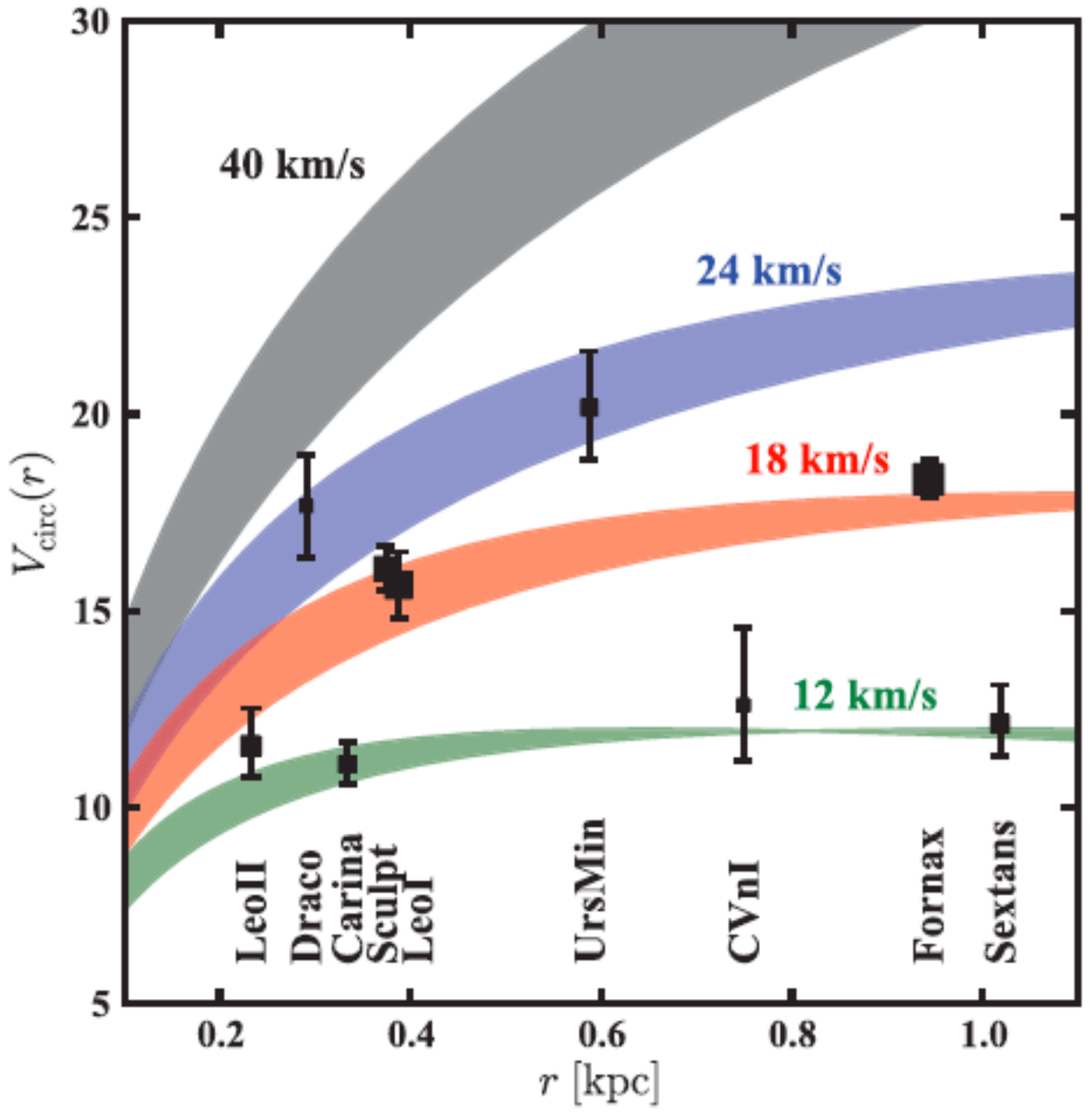

Figure 1. Observed $V_{\rm circ}$ values of the nine bright dSphs (symbols, with sizes proportional to log L_V), along with rotation curves corresponding to NFW subhaloes with $V_{\rm max} = (12, 18, 24, 40)\,{\rm km\,s^{-1}}$. The shading indicates the 1σ scatter in $r_{\rm max}$ at fixed $V_{\rm max}$ taken from the Aquarius simulations. All of the bright dSphs are consistent with subhaloes having $V_{\rm max} \leq 24\,{\rm km\,s^{-1}}$, and most require $V_{\rm max} \lesssim 18\,{\rm km\,s^{-1}}$. Only Draco, the least luminous dSph in our sample, is consistent (within 2σ) with a massive CDM subhalo of $\approx$40 km s^{-1} at $z = 0$.

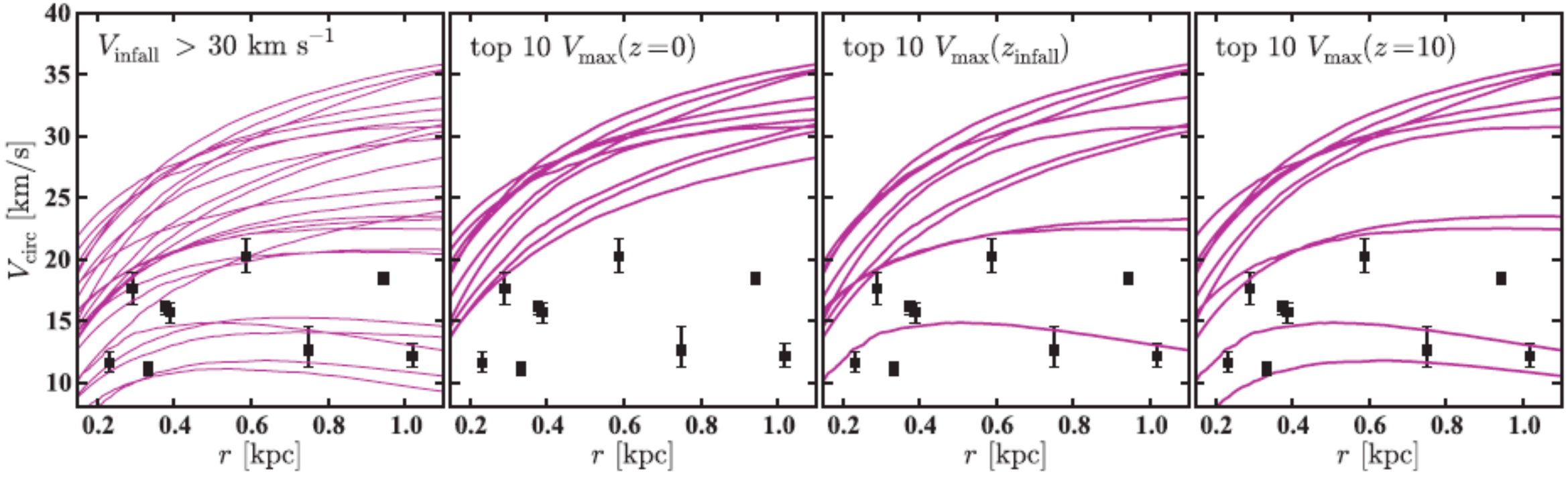

Left-hand panels: circular velocity profiles at redshift zero for subhaloes of the Aquarius halo (M*v*ir = 1.4 x 10^{12} M) that have $V_{infall} > 30$ km s^{-1} and $V_{max}(z = 0) > 10$ km s^{-1} (excluding Magellanic Clouds candidates).

Measured $V_{circ}(r1/2)$ values for the MW dSphs are plotted as data points with error bars. Each subsequent panel shows redshift-zero rotation curves for subhaloes from the left-hand panel with the 10 highest values of $V_{max}(z = 0)$ (second panel), V_{infall} (third panel) or $V_{max}(z = 10)$ (fourth panel). In none of the three scenarios are the most massive subhaloes dynamically consistent with the bright MW dSphs: there are always several subhaloes more massive than all of the MW dSphs. (Analogous results are found for the other four haloes.)

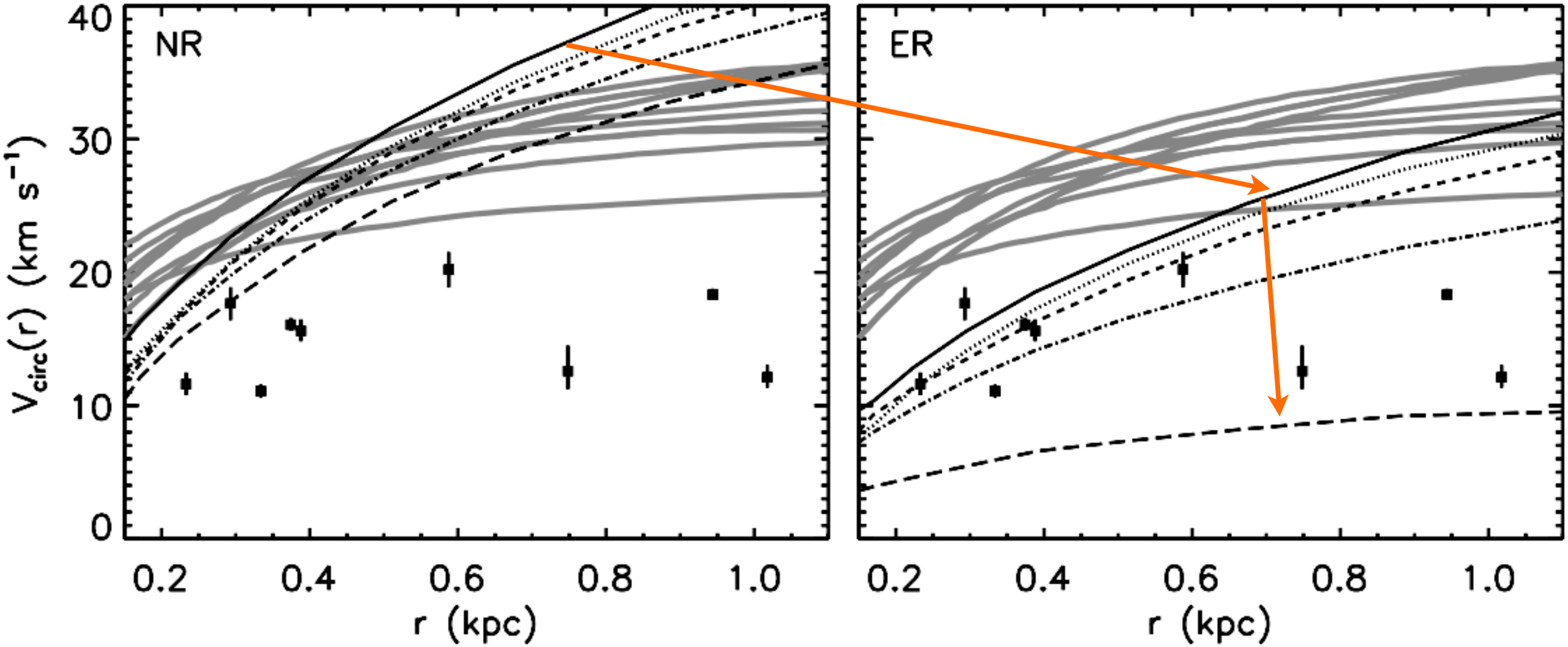

Comparison of circular orbits to observations of the MW satellites (black squares) and the Aquarius E halo's "massive failures" from the analysis of Boylan-Kolchin et al. (2012) (thick grey lines). Left: The circular velocity profiles of the no mass removal case (NR). This profile does not agree with the MW dSph population and was created to mimic the Aquarius cosmological simulations. Right: The circular velocity profiles of the exponential mass removal case (ER). These profiles span a much larger range of parameter space and are in agreement with observed MW dwarfs due to their inclusion of baryonic effects. Both panels show the initial isolated profile as a solid black line. The circular orbits after 5 Gyrs of evolution are shown from top to bottom as:

150 kpc (dotted), 100 kpc (short-dashed), 70 kpc (dash-dotted), and 50 kpc (long-dashed).

K. Arraki et al ApJ 2012